

# Evaluation of Cu-OFP Creep Crack Growth and Theoretical Fracture Models for Cu-OFP

**Anders Björkblad**  
**Jonas Faleskog**

POSIVA OY

Olkiluoto  
FI-27160 Eurajoki, Finland  
Phone +358 2 8372 31  
posiva.fi

SVENSK KÄRNBRÄNSLEHANTERING AB

SWEDISH NUCLEAR FUEL  
AND WASTE MANAGEMENT CO

Box 3091, SE-169 03 Solna  
Phone +46 8 459 84 00  
skb.se



ISSN 2489-2742

**Posiva SKB Report 03**

SKB ID 1519789

Posiva ID RDOC-104826

November 2018

# **Evaluation of Cu-OFP Creep Crack Growth and Theoretical Fracture Models for Cu-OFP**

Anders Björkblad, Swerea KIMAB AB

Jonas Faleskog, KTH

This report concerns a study which was conducted for Svensk Kärnbränslehantering AB (SKB) and Posiva Oy. The conclusions and viewpoints presented in the report are those of the authors. SKB or Posiva may draw modified conclusions, based on additional literature sources and/or expert opinions.

A pdf version of this document can be downloaded from [www.skb.se](http://www.skb.se) or [www.posiva.fi](http://www.posiva.fi).

© 2018 Svensk Kärnbränslehantering AB and Posiva Oy



## Summary

The creep properties of phosphorus-alloyed oxygen-free copper (Cu-OFP) have been investigated in a series of uni-axial creep test and creep crack growth (CCG) tests performed at room temperature and at temperatures as high as 215 °C. The duration of the tests was in the range of 300–20 000 h. All tests were conducted in the laboratory of Swerea KIMAB during the period of 1997–2014. The uni-axial tests were carried out on various round and flat tensile specimens and the CCG tests were conducted on compact tension (CT) specimens with a spark-eroded notch. The notch radius was 0.2 mm. There has been a renewal of interest to revisit these tests and to examine the Cu-OFP material subjected to various extents of creep deformation for the purpose of identifying the type of damage that has occurred in Cu-OFP and to characterize the incipient crack growth that can be observed at the highest temperature. The result from this new examination is presented in this report. This examination was carried out by an appropriate sectioning of the material and thereafter careful examination in SEM. To support the findings of this examination, a literature survey was conducted. The focus of this survey was on failure mechanisms in Cu that is relevant to the experimental studies discussed above. Another object of interest in the work was load cases affecting the copper canister in the final disposal of spent nuclear fuel used in Sweden and Finland. Here, two load cases were considered: relatively rapid loading at room temperature and below and constant external pressure at approximately 100 °C over thousands of years. The survey suggests that copper will fail by ductile fracture at room temperature, essentially insensitive to the rate of loading if strain rates are below  $10^3 \text{ s}^{-1}$ . Creep deformation of copper at about 100 °C can be expected to be extremely slow at the studied load cases, where a possible mechanism for creep deformation would be due to cavities located at grain boundaries that grow by surface diffusion coupled to power law creep.

## Sammanfattning

Krypegenskaperna hos syrefri koppar med fosforstillsats (Cu-OFP) har undersökts i en serie enaxliga prover samt i prover för att studera tillväxt av krypsprickor (creep crack growth, CCG) utförda vid rumstemperatur och vid temperaturer så höga som 215 °C. De olika proven har pågått under tider i intervallet 300–20 000 timmar. Alla prover har utförts i kryplaboratoriet hos Swerea KIMAB under perioden 1997–2014. De enaxliga proven utfördes med olika runda och platta dragprovstavar, och CCG-proverna utfördes med så kallade compact tension-provstavar (CT) med anvisningar som skapats med trådgnistning. Anvisningens radie var 0,2 mm. Ett förnyat intresse har uppstått att gå tillbaka till resultat från dessa försök och undersöka Cu-OFP-materialet som har utsatts för olika former för krypdeformation, med syfte att identifiera den typ av skada som har uppstått i Cu-OFP och karakterisera den begynnande spricktillväxt som kan observeras vid den högsta temperaturen. Resultaten från denna nya undersökning presenteras i föreliggande rapport. Denna undersökning utfördes genom en lämplig sektionering av materialet och därefter noggrann undersökning med svepelektronmikroskop (SEM). För att stötta resultaten av denna undersökning genomfördes en litteraturundersökning. Denna studie fokuserades på de brottmekanismer i Cu som är relevanta för de experimentella studier som beskrivits ovan. Ett andra fokus var de lastfall som påverkar kopparkapseln i slutförvaret av använt kärnbränsle i Sverige och Finland. Här betraktades två lastfall: relativt snabb belastning vid rumstemperatur eller lägre samt konstant yttre tryck vid ungefär 100 °C under tusentals år. Undersökningen tyder på att koppar kommer att brista duktilt vid rumstemperatur, huvudsakligen okänsligt för belastningshastigheten om töjningshastigheten är under  $10^3 \text{ s}^{-1}$ . Krypdeformation av koppar vid cirka 100 °C kan förväntas vara extremt långsamt vid de undersökta lastfallen, där en möjlig mekanism för krypdeformation skulle bero på kaviteter som finns vid korngränser och som växer genom ytdiffusion kopplad till krypning som kan beskrivas av en matematisk potensfunktion.

## Tiivistelmä

Fosforiseostetun hapettoman kuparin (Cu-OFP) virumisominaisuuksia on tutkittu huoneenlämpötilassa sekä korotetuissa lämpötiloissa aina 215 °C asti suoritetuissa yksiaksiaalisissa virumiskokeissa ja virumissärönkasvukokeissa (creep crack growth, CCG). Kokeiden kesto-aika vaihteli välillä 300 h–20 000 h. Kaikki kokeet suoritettiin Swerea KIMAB:n laboratoriossa vuosien 1997 ja 2014 välillä. Yksiaksiaaliset virumiskokeet tehtiin erilaisilla pyöreillä sekä litteillä vetosauvoilla ja virumissärönkasvukokeet tehtiin CT-sauvoilla, joihin oli tehty 0,2 mm säteellä oleva kipinätyöstetty lovi. Nyt on ilmennyt kiinnostusta tarkastella koetuloksia sekä kokeissa käytettyä Cu-OFP materiaalia uudestaan. Uuden tarkastelun tarkoituksena on selvittää koesauvoista, joihin on aiheutettu erisuuruisia virumismuodonmuutoksia, minkälaista vauriota materiaalissa on tapahtunut sekä karakterisoida suurimmassa lämpötilassa testatuissa koesauvoissa havaittu alkava särönkasvu. Tämä raportti esittää tämän uuden tarkastelun tulokset. Tarkastelussa tutkittiin soveltuviin paloihin pilkottuja koesauvoja tarkasti SEM-elektronimikroskoopilla. Tarkastelun tueksi tehtiin kirjallisuustutkimus, jonka kohteena olivat tarkastelun alla olevien kokeiden kannalta oleelliset vauriomekanismit. Työn toinen kiinnostuksen kohde oli kuormitustapaukset, jotka vaikuttavat käytetyn ydinpolttoaineen loppusijoituksessa Ruotsissa ja Suomessa käytettyyn kuparikapseliin. Työssä käsiteltiin kahta kuormitustapausta: huoneenlämpötilassa tai sitä viileämmässä tapahtuva suhteellisen nopea kuormitus sekä 100 °C:ssa yli tuhansien vuosien ajan vaikuttava vakiosuuruinen ulkoinen paine. Selvityksen perustella kuparin murtumismekanismi huoneenlämpötilassa on sitkeä särönkasvu ja vaurio on käytännössä kuormitusnopeudesta riippumaton, jos venymänopeudet ovat alle  $10^3 \text{ s}^{-1}$ . Voidaan odottaa, että tarkastelluissa kuormitustapauksissa kuparin virumismuodonmuutos noin 100 °C:n lämpötilassa on äärimmäisen hidasta ja virumismuodonmuutoksen mahdollinen vaikutusmekanismi on raerajoilla sijaitsevien sulkeumien kasvu, joka tapahtuu pintadiffuusion sekä Power Law – virumisen kautta.



# Contents

<b>1</b>	<b>Introduction</b>	9
1.1	Background	9
1.2	Nomenclature—cracks and crack formation in CCG	10
1.3	Objectives	10
<b>2</b>	<b>Fracture models for Cu-OFP—A literature survey</b>	11
2.1	Scope and limitations	11
2.2	Mechanical properties of the material in the copper canisters	12
2.3	Plastic flow ahead of a blunted crack tip	12
2.4	Case ( <i>i</i> ): slow to high rate loading at room temperature and below	13
2.5	Case ( <i>ii</i> ): constant pressure loading at approximately 100 °C	14
2.6	Intergranular creep fracture—the critical mode of failure	16
2.7	Summary of fracture models for Cu-OFP	17
<b>3</b>	<b>Background data—previous testing</b>	19
<b>4</b>	<b>Review of previous creep crack growth testing on Cu-OFP</b>	23
4.1	Results from previous testing	23
4.2	Fracture surface appearance of a regular uniaxial creep test in OFP copper	23
4.3	Cut-up views from CCG CT specimens	27
4.3.1	View A–A from specimen no 1 (T = 100 °C, $\sigma_{\text{ref}} = 185$ MPa)	28
4.3.2	View A–A from specimen no 2 (T = 125 °C, $\sigma_{\text{ref}} = 165$ MPa)	29
4.3.3	View A–A from specimen no 3 (T = 175 °C, $\sigma_{\text{ref}} = 115$ MPa)	29
4.3.4	View A–A from specimen no 4 (T = 125 °C, $\sigma_{\text{ref}} = 165$ MPa)	29
4.3.5	View A–A from specimen no 5 (T = 125 °C, $\sigma_{\text{ref}} = 165$ MPa)	31
4.3.6	View C–C from specimen no 6 (T = 75 °C, $\sigma_{\text{ref}} = 165$ MPa)	31
4.3.7	View B–B from specimen no 7 (T = 125 °C, $\sigma_{\text{ref}} = 165$ MPa, separated in halves)	35
<b>5</b>	<b>Discussion and conclusion</b>	39
	<b>References</b>	41



# 1 Introduction

## 1.1 Background

Phosphorus-alloyed oxygen-free copper (Cu-OFP) with a 5 cm wall thickness are planned to be used for the outer corrosion barrier of the KBS-3 canister with a load bearing nodular cast iron insert for final disposal of spent nuclear fuel in the Swedish and Finnish nuclear waste programme. It is estimated that during the first few hundred years of service the Cu-OFP shell of the canisters will be exposed to external pressures as high as 15 MPa and temperatures up to approximately 100 °C in the repository (Raiko et al. 2010). These conditions will cause creep deformation in the Cu-OFP.

The Cu-OFP canister will be exposed to multiaxial stress states when external hydrostatic pressure and swelling pressure from the surrounding bentonite is developed. It is well known that multiaxiality can have a strong effect on the ductility of materials. Under high degrees of tensile multiaxiality, ductility will decrease remarkably for notch-sensitive materials, leading to premature failure. High degrees of multiaxiality can be found especially at notch roots or in front of crack tips. Cu-OFP appears to be the most suitable candidate canister material (Seitisleam and Henderson 1997, Andersson et al. 1999, Sandström and Wu 2007). Although the creep ductility of Cu-OFP is high, a crack growing under multiaxial stress states during creep might lead to premature failure.

At temperatures ranging from 0 to 100 °C, Cu-OFP is very ductile under monotonically increasing loading at rates that lead to fracture in less than approximately 1 h. It is impossible to carry out a fracture test on Cu-OFP under conditions of linear elastic fracture mechanics (LEFM) with reasonably sized specimens (Anderson 2005). It is also very difficult to carry out testing resorting to a nonlinear fracture mechanics (NLFM) theory because of the extensive crack tip blunting that occurs during a fracture test. For a standard sized compact tension (CT) specimen ( $W = 50$  mm), the crack tip blunting soon becomes so severe that it more resembles a uniaxial tensile test. A valid (NLFM) fracture toughness test would require a very large specimen (in the region of 500–800 mm of width), owing to the low initial yield stress in Cu-OFP combined with high toughness.

For decreased rates of loading, which allow for a possible creep mechanism, the conditions under which failure can occur remain unclear. For instance, is it possible to achieve crack growth in a CT-test that has been loaded to a certain level high in the nonlinear regime and then kept constant if the time is sufficiently long? In such a CT-test, it is typical for the crack to no longer be characterized as a sharp crack but rather as blunted notch defined by its opening. The size of the notch opening determines the length scale of the deformation process and the amount of material that will be subjected to high stresses and strains.

It is currently unclear whether Cu-OFP shows crack propagation behaviour according to regular fracture mechanics or some type of creep fracture emanating from a blunted notch when exposed to a sustained load at the temperatures in focus. Despite a substantial amount of creep and creep crack growth (CCG) testing, a clear picture of the crack behaviour of Cu-OFP has yet to be established.

CCG testing under a multiaxial stress state using CT specimens has been conducted at Swerea KIMAB during the period of 1997–2014. The testing has been focused mainly at temperatures between room temperature (RT) and 125 °C. A few tests were performed at 175–215 °C as well; however, it should be observed that this temperature range is outside the specification for the final disposal. Time perspectives for the accomplished testing are in the range of 300–20 000 h. The purpose of this investigation was to compile the gathered result from those tests from a fracture mechanics perspective and to search the literature for experimental observations and models of relevance for the load conditions under the range of temperatures the Cu-OFP canister may encounter in the deep geological repository.

## **1.2 Nomenclature—cracks and crack formation in CCG**

The meaning of cracks and crack establishment was of crucial interest for this investigation. Normally, when referring to cracks in engineering materials, cracking from a fracture mechanics point of view are understood to have (theoretically) infinitely sharp crack tips (Anderson 2005). However, for Cu-OFP within this study, this is not the case. The radius of the blunted notches in the CT specimens used for the CCG testing is in the range of millimetres. Moreover, cracks that initiate at bottom of the notch show an immediate blunting. Crack formation has been observed via void growth coalescence and shear localization, but the growth has, in all cases, originated from extensively strained and blunted notches. Thus, the crack growth observed in the present investigation is solely of a ductile nature, and the final failure is essentially related to a slow tensile fracture or evolving creep damage. This finding also implies that the normal picture of a crack as something of immediate danger is not necessary valid for Cu-OFP.

Therefore, it appears suitable to introduce a distinction between “normal” crack formation and creep crack formation in Cu-OFP. Consequently, the discussion of cracks and crack growth in this report (excluded “Background material—previous testing” below) refers to the non-brittle, tough fracture behaviour of Cu-OFP described above.

## **1.3 Objectives**

The scope of the present work was to critically review earlier CCG testing in Cu-OFP performed at Swerea KIMAB. Of primary focus was to investigate whether evidence of crack initiation or crack growth could be found in the CCG tests performed. For this purpose, the previously tested CT specimens were cut up again in new virgin planes and directions so that traces of creep and fracture mechanisms could be re-examined. No other attention was paid to the earlier testing.

In support of this fractographic investigation, a limited literary survey was performed. Of key interest in this survey was to find possible fracture mechanisms to explain the observations made.

## 2 Fracture models for Cu-OFP—A literature survey

### 2.1 Scope and limitations

To limit the scope of this literature study, a short account of the type of loading a copper canister will be subjected to will be given, see also Raiko et al. (2010). Initially, when the radioactive waste is deposited into the canister and placed in the deep geological repository, the temperature will rise to approximately 100 °C. The copper canister will be subjected to an external pressure owing to ground water hydrostatic pressure and swelling of the bentonite buffer, which will close the gap between the copper canister and the insert of nodular cast iron over a period that can range from a few hundred years to several thousand years. The temperature will decay and is expected to be in the range of 0 °C to 20 °C when 20 000 years have passed. The canister may also be subjected to rapid shear loading caused by earthquakes owing to the release of tectonic forces from isostatic rebound of the lithosphere. Even though the geographic location of the repository is chosen to minimize the risk of earthquakes, the risk of earthquakes will increase after 50 to 60 thousand years due to an expected future glaciation. To summarize: (i) the copper canister will be subjected to a static loading of an isostatic pressure at a temperature of approximately 100 °C; (ii) the copper canister is at risk to be subjected to a rapid loading event, which if it occurs, most likely will occur at a temperature in the range 0 °C to 20 °C.

Generally, copper will deform elastically at low stress levels and at low temperatures. At higher levels of stress, copper can deform by irreversible dislocation plasticity or, if the temperature is sufficiently high, by diffusional flow or power-law creep. Creep phenomena are generally assumed to be present in metals at temperatures above about  $0.3 \cdot T_m$ , where  $T_m$  is the melting temperature, which is equal to 1 356 K (1 084 °C) in the case of copper. The interplay between stress and temperature can be summarized in a so-called “deformation mechanism map” as introduced by Ashby et al. (1979). Such a diagram was constructed for oxygen-free high conductivity (OFHC) copper in Ashby et al. (1979) based on a number of experiments conducted at low to high temperatures, as discussed next. At low temperatures copper fail by ductile failure (Carrecker and Hibbard 1953, Greenwood et al. 1954). At temperatures above 180 °C, copper creeps and fails by transgranular creep fracture if the creep strain rate is sufficiently high enough; otherwise, failure occurs by intergranular fracture (Fleck et al. 1970, Hull and Rimmer 1959, Jenkins and Digges 1950).

Based on the discussion above, this literature survey is limited to the following cases: (i) ductile failure at low temperature under slow to fast strain rate loading conditions; and (ii) possible creep fracture at relatively low temperatures (approximately 100 °C) under constant pressure acting on the canister due to the increased pressure prevailing in the deep geological repository compared with ground level. These two cases will be addressed below.

In both the cases discussed above failure would ultimately be ductile in nature, and ductile failure is sensitive to the type of stress state that prevails. In particular the stress triaxiality has a profound effect on the strain to failure. Stress triaxiality is defined by  $T = \sigma_m / \sigma_e$ , where  $\sigma_m$  is the mean stress and  $\sigma_e$  is the von Mises effective stress. For instance,  $T = 1/3$  under conditions of uniaxial tension. A higher triaxiality can be obtained by introducing a notch into the test geometry. For instance, by providing a smooth round bar specimen (diameter  $2r$ ) with a notch having a local root radius  $R$ , triaxiality will increase according to Bridgman correction:

$$T = \frac{1}{3} + \ln \left( 1 + \frac{R}{2r} \right) \quad \text{Equation 2-1}$$

As an example,  $a/R = 0.2$  and  $0.8$  result in  $T = 0.43$  and  $0.67$ .

## 2.2 Mechanical properties of the material in the copper canisters

The copper canisters will be manufactured from oxygen free pure copper micro-alloyed with phosphorous, Cu-0FP. The material will be used in an annealed condition (annealed during hot working) and is studied and characterized in Sandström et al. (2009), where uniaxial test data pertaining to temperatures in the interval of 20 to 175 °C and strain rates in the range  $10^{-7}$  to  $10^{-1}$  s<sup>-1</sup> are presented. Figure 2-1 shows engineering stress–strain curves from slow uniaxial tensile tests at 20 °C, 75 °C and 125 °C in (a), (b) and (c), respectively, and the initial yield strength (0.2 % proof stress) versus temperature for tests performed in the strain-rate interval of  $10^{-4}$  to  $10^{-7}$ . Note that material exhibits a very strong strain hardening, with an ultimate tensile strength more than 2.5 times the initial yield strength of the material, where the true ultimate stress ( $\sigma_{\text{true}} = \sigma_{\text{eng}}[1 + \epsilon_{\text{eng}}]$ ) is greater than 230 MPa. The shear modulus is also reported in Sandström et al. (2009), and changes from 42.5 GPa to 40.7 GPa when the temperature increases from 20 °C to 125 °C. A Poisson’s ratio of  $0.33 \pm 0.03$  is commonly reported in the literature. By assuming isotropic behaviour in copper, the elastic modulus changes from  $113.0 \pm 2.5$  GPa to  $108.3 \pm 2.5$  GPa when the temperature increases from 20 °C to 125 °C.

## 2.3 Plastic flow ahead of a blunted crack tip

All pre-cracked specimens scrutinized in this report have been subjected to substantial plastic deformation due to loading in the beginning of the creep tests. Thus, the notch fronts in these specimens features a highly strained notch section at the onset of the creep test. To give a few examples, the cut up views of the CT specimens shown in Sections 4.3 belong to specimens with a blunted notch tip radius in the range of millimetres. The initiation of crack like defects at a blunted notch tip is likely to follow paths of intense plastic yielding. A simple way to construct such paths is by the use of the slip line theory. Rice and Tracy (1969) present a slip line field solution near a blunted crack tip. For the special case of a crack tip blunting into a shape of a semi-circle of diameter  $\delta_i$ , the region ahead of the crack would have exponential spiral slip lines and would extend a distance  $(\exp(\pi/2) - 1)\delta_i/2 \approx 1.9\delta_i$ . The slip line field belonging to a blunted crack tip of semi-circular shape is displayed in Figure 2-2.

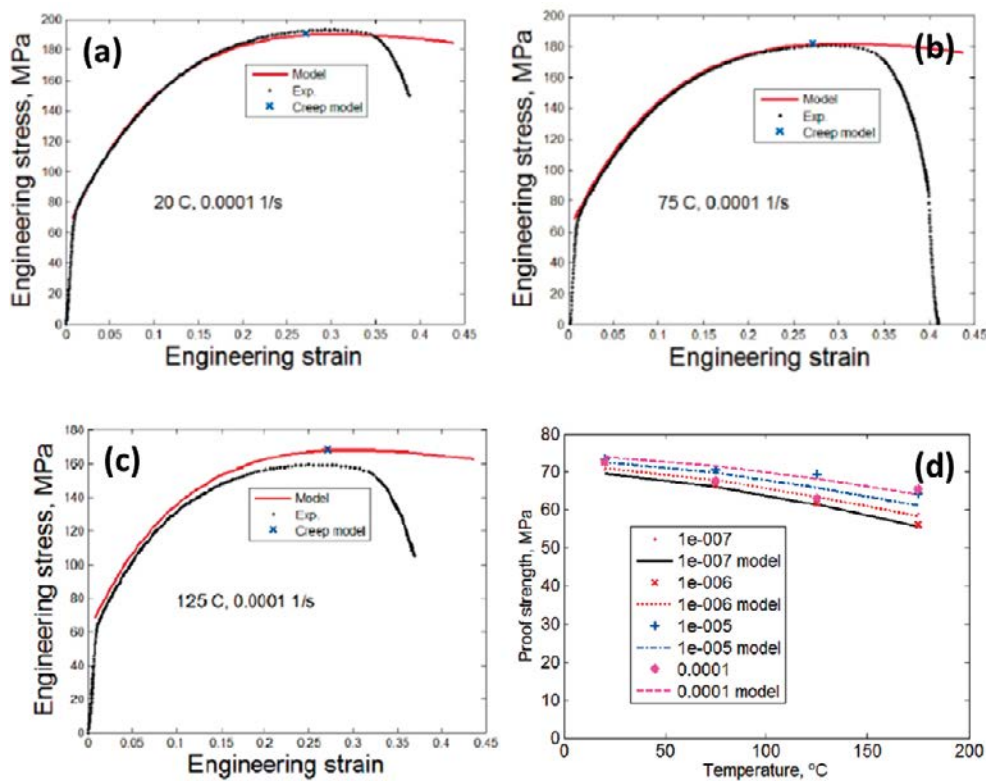


**Figure 2-1.** Uniaxial engineering stress–strain curves for Cu-0FP at (a) 20 °C, (b) 75 °C and (c) 125 °C. The initial yield stress (0.2 % proof stress) versus temperature from tests performed with different strain rates are shown in (d), where the symbols represent experimental data. All data are taken from Sandström et al. (2009).

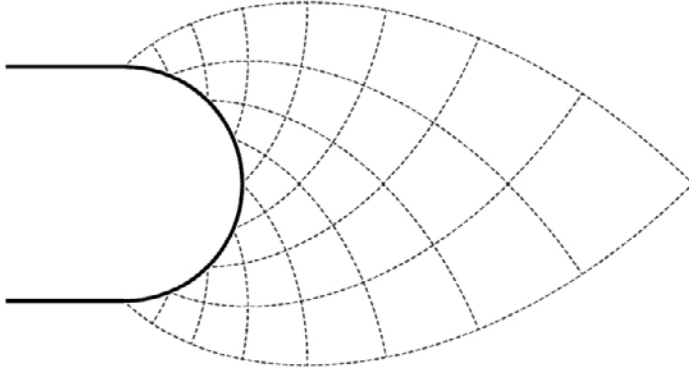


**Figure 2-2.** A slip line field solution ahead of a crack tip that has blunted into a semicircle (solid line) is described by exponential spiral slip lines as depicted by the dashed lines.

## 2.4 Case (i): slow to high rate loading at room temperature and below

If the copper canister is subjected to rapid loading at room temperature and below, it will most likely fail by ductile fracture. Copper is very ductile at room temperature. For instance, the area reduction in uniaxial tests of Cu-OFP is 80 to 90 percent (Andersson 2005), and it is virtually impossible to carry out a valid fracture mechanics test using standard specimen geometries.

Notable experiments have been carried out on copper at room temperature. Pardoen and Delannay (1998) and Pardoen et al. (1998) performed tests on smooth and notched round bar specimens of cold-drawn 99.97 percent pure copper. The copper material they investigate has a similar uniaxial stress-strain response as the Cu-OFP of interest to SKB (Sandström et al. 2009). Pardoen and co-workers developed a special technique to measure the void volume fraction and its progression in the material upon loading. Voids nucleate around a fine dispersion of ellipsoidal copper oxide inclusions (1 to 2 microns in size) contained in the copper matrix. The material fails when these voids grow and coalesce. Due to the simple nature of the tests, the mechanical state in the material in terms of stresses, equivalent plastic strain and void volume fraction can be evaluated in each test. The information is used to check the validity of several established models for void growth, such as the micromechanical model by Rice and Tracy (1969) and the continuum damage models by Gurson (1977), as enhanced by Tvergaard (1981) and Gologanu et al. (1997). Below, these models are denoted as RT-, GT- and GLD-model, respectively. According to the RT model, the growth rate of a spherical void with radius  $R_v$  is given by

$$\frac{\dot{R}_v}{R_v} = \alpha \exp\left(\frac{1.5\sigma_m}{\sigma_e}\right) \dot{\bar{\epsilon}}, \quad \text{Equation 2-2}$$

where  $\alpha = 0.427$  is a constant (Huang 1991) and  $\dot{\bar{\epsilon}}$  is the equivalent plastic strain rate, and the stress measures  $\sigma_m$  and  $\sigma_e$  represents the mean stress and the effective von Mises stress, respectively, where the ratio denote stress triaxiality as discussed in Section 2.1. The behaviour of the continuum type models, GT and GLD, are governed by their yield functions, which may be written as

$$\Phi = \left(\frac{\sigma_e}{\Sigma_1}\right)^2 + 2qf \cosh\left(\frac{3\sigma_m}{2\Sigma_2}\right) - (1 + (qf)^2) = 0 \quad \text{and} \quad \dot{f} = (1 - f)\dot{\epsilon}_{kk}^p, \quad \text{Equation 2-3}$$

where  $f$  is void volume fraction,  $q$  is a fitting (material) parameter, and  $\dot{\epsilon}_{ij}^p$  are the components of the plastic strain rate tensor and thus  $\dot{\epsilon}_{kk}^p$  represents the rate of plastic volume change. For the GLD-model, the functions:  $\Sigma_1 = \Sigma_1(f_0, E_m, E_e)$  and  $\Sigma_2 = \Sigma_2(f_0, E_m, E_e)$ , and for the GT-model the functions:  $\Sigma_1 = \Sigma_2 = \bar{\sigma}$ . Here,  $E_m$  and  $E_e$  are two overall hardening parameters that depends on the deviatoric and hydrostatic parts of the aggregate strain rate, respectively, and  $\bar{\sigma}$  is the flow stress of the matrix material. Pardoen and co-workers tested these models against experimental data and found that predictions of void volume fraction from the RT-model agree fairly well with experimental data. Also, the corresponding predictions from the GT- and GLD-models agree fairly well with the experimental data, where the GLD-model is slightly better owing to its ability to account for a non-spherical void shape.

Mirza et al. (1997) carried out experiments on OFHC copper of purity 99.95 % using smooth and notched round bar test specimen. The objective was to investigate the effects of stress triaxiality and loading rate on the various stages of ductile failure and fracture. The tests were carried out at room temperature with strain rates up to  $0.2 \text{ s}^{-1}$ , which is in the vicinity of the strain rate that may occur in the copper canister when subjected to rapid shear loading from earthquakes. For all tests, Mirza et al. (1997) observed that material failure occurs by ductile fracture by void nucleation, growth and coalescence. The initiation of visible cracks occurs at strain levels (logarithmic strains locally) of approximately 1.5 in the plane sided specimen (stress triaxiality,  $T \approx 0.33$ ) and at approximately half of that, 0.7, in plane sided specimen with a rather sharp notch ( $T \approx 1.5$ ). Moreover, the influence of strain rate on the failure process is insignificant. Additionally, Lassila (1989) and Parry and Walker (1989), reported that strain rates up to  $10^3$ , has essentially no influence on ductile fracture in copper.

To summarize this section: at room temperature and below, Cu-OFP will fail by ductile fracture. This mode of failure seems to be insensitive to loading rates in the range of interest for the rapid shear loading to which a canister may be subjected during an earthquake. Well established models for ductile failure by void growth and coalescence seem to work well.

## 2.5 Case (ii): constant pressure loading at approximately 100 °C

The hydrostatic pressure acting on the copper canister is expected to change over time. Over the first tens of thousands years, the hydrostatic pressure is estimated to reach approximately 15 MPa, and is mostly due to the bentonite swelling (Raiko et al. 2010). The copper canister is a cylinder with a mean radius of 500 mm and a thickness of 49 mm. A simple stress analysis based on the thin wall approximation suggests that a state close to generalized plane strain would prevail in the wall of the canister, in which the normal stress in the circumferential direction would be approximately ten times the hydrostatic pressure i.e., equal to  $-150 \text{ MPa}$ . The normal stress in the axial direction would be half the value in the circumferential direction and the normal stress in the radial direction would be approximately one tenth. Thus, the von Mises effective stress then becomes 0.87 times the circumferential stress i.e.,  $130 \text{ MPa}$ . This is much larger than the initial yield stress of the Cu-OFP material as seen in Figure 2-1(a) but well below the ultimate tensile strength ( $>180 \text{ MPa}$ , nominal stress). The gap between the canister and the insert of nodular cast iron is approximately 1 mm in the radial direction. Hence, the gap will be closed if the copper canister is subjected to a normal strain in the circumferential direction corresponding to  $-0.002$ , which is very small. In fact, when the hydrostatic pressure slowly increase around the copper canister to reach 15 MPa, plastic deformation alone will suffice to close the gap between the canister and the insert, as is clearly seen from stress–strain relations in Figure 2-1. Thus, the possible contribution of creep would merely be to speed up the closure of the gap, and after closure relax the stresses in the copper canister. However, it should be pointed out that in the regions where the top and bottom lids are welded to the copper canister, substantially higher inelastic strains are expected to arise at highly localized spots. But again, these will arise in compressive stress fields.

As discussed above, Ashby et al. (1979) presented results suggesting that copper would not deform by a creep mechanism at temperatures as low as 100 °C or lower. However, some experimental studies indicate that this finding may not be entirely true. Yagodzinskyy et al. (2012) carried out uniaxial tensile tests at 50 °C ( $\approx 0.24T_m$ ) in distilled water on flat specimens of OFP copper of nominal purity 99.992 %, containing less than 2 wt. ppm of oxygen and approximately 50 wt. ppm of phosphorus. The OFP copper considered by Yagodzinskyy et al. (2012), is a highly strain hardening material with a yield stress of around 30 MPa and an ultimate tensile strength near 160 MPa (nominal stress). The specimens were loaded at a constant strain rate of  $10^{-4} \text{ s}^{-1}$  to the desired load corresponding to nominal stresses in the range 80 MPa to 140 MPa, with related nominal strains in the range 0.08 to 0.20. Hence, the true normal stresses in these tests were consequently higher. Nevertheless, of interest here is that a very small but detectable second stage creep strain rate was observed in the tests. The data were fitted to a Norton creep relation, which resulted in an exponent of approximately 3.3 for an applied stress greater than 100 MPa. However, no creep rupture was observed throughout the tests. Yagodzinskyy et al. (2012) also performed the same type of tests as described above on hydrogen charged specimens and observed an increased creep strain rate.

The relation between strain rate and stress depends on temperature, time and some effective measure of stress. For many metals, including copper, a simple phenomenological power-law expression of the form

$$\dot{\bar{\epsilon}} = A \left( \frac{\bar{\sigma}}{\sigma_0} \right)^n, \quad \text{Equation 2-4}$$

seems to capture the observed stress–strain rate response well in the secondary stage provided that the applied stress is neither too small nor too large. Here,  $\dot{\bar{\epsilon}}$  is an equivalent strain rate (equal to the normal strain rate in a uniaxial test),  $\bar{\sigma}$  is an effective measure of stress, typically the von Mises effective stress (equal to the normal stress in a uniaxial test),  $n$  is an exponent that to some extent depends on the stress level,  $\sigma_0$  is a reference stress, and  $A$  is a material parameter that depends on temperature and seems to follow an Arrhenius relation  $A = \exp(-Q_c/(RT))$ , where  $Q_c$  is the activation energy for creep,  $R$  is the universal gas constant, and  $T$  is the temperature. For multiaxial conditions, the creep strain components may be written as

$$\dot{\epsilon}_{ij}^c = \dot{\bar{\epsilon}} \frac{\partial f}{\partial \sigma_{ij}}, \quad \text{Equation 2-5}$$

where  $\dot{\bar{\epsilon}}$  is defined in Sandström and Wu (2007) and the plastic creep directions are given as the gradient to a load function  $f$ , often of the von Mises type i.e.,  $\partial f / \partial \sigma_{ij} = 3s_{ij} / (2\sigma_e)$ . Equation (2-5) is written using index notation, where the indices  $i$  and  $j$  refers to components in three-dimensional Euclidean space.

Wilshire and Battenbough (2007) discuss the difficulty of using laboratory test results obtained over a relatively short time to estimate parameters in a creep constitutive equation to be used to predict the creep response over a much larger time span. To accelerate the testing in the laboratory, testing is typically performed at considerably higher levels of stress or at a higher temperature. A problem related to this is that the exponent in Sandström and Wu (2007) depends on the level of stress. In many pure metals the exponent is roughly equal to 4 over stress ranges where creep rates can be measured easily. At high stress levels the power-law behaviour in Sandström and Wu (2007) breaks down and the strain rate seems to instead depend exponentially on stress. Moreover, at low stress levels, the exponent  $n$  decreases towards unity, and this change in response is usually attributed to a change from the dislocation creep process to diffusional creep mechanisms, as also discussed by Cocks and Ashby (1982) and more recently by Wilshire and Battenbough (2007).

Creep fracture may occur by transgranular or intergranular fracture. *Transgranular creep fracture* is very similar to low-temperature ductile fracture, in which holes nucleate and grow until they coalesce to create a fracture path. Creep deformation may affect this failure process in two ways: first, creeping tend to lower the stresses at stress concentrations such as notches and nucleation may be postponed to higher levels of strains; second, the strain rate dependence of creep can stabilize flow and delay void coalescence. *Intergranular creep fracture* is primarily observed at lower levels of stress, and longer times-to-fracture. Here, grain boundaries slide and voids grow and link up to form micro-cracks at grain boundaries. The time-to-fracture  $t_f$  and the equivalent strain-rate are related as  $t_f \dot{\bar{\epsilon}} = C$ , for many metals, including copper, where  $C$  is a constant over limited ranges of stress and temperature under steady state conditions. This relation, reported by Monkman and Grant (1956) based on experimental observations, suggests that fracture would be controlled by power-law creep and not by a diffusion process. However, there are several possible explanations for the simple nature of the expression: void or crack nucleation is controlled by power-law creep and consumes almost all life of the specimen; or the nucleated voids are small, they grow by local diffusion, in which the rate of diffusion is controlled by power-law creep in the surrounding grains. Growth of voids and micro-cracks is then a result of coupled diffusion and power-law creep. This mechanism is more severe than transgranular creep fracture because the progression of damage is confined to grain boundaries, and failure of a structure may occur without any larger overall strain. Therefore, intergranular creep fracture will be further discussed in the next sub-section.

## 2.6 Intergranular creep fracture—the critical mode of failure

The models for creep fracture discussed so far are phenomenological in nature. A number of studies have developed and proposed mechanism based continuum material damage models for intergranular creep fracture suitable for computational studies by the finite element method. Cocks and Ashby (1982) presented a pioneering work comprising a comprehensive study of mechanism based models for creep fracture by void (cavity) growth. Their focus was on damage located on grain boundaries and considered progressive damage due to void growth controlled by boundary diffusion, or surface diffusion (that involves void surfaces), or power-law creep or a combination thereof in pairs. Void growth maps are constructed in which the controlling void growth mechanisms are given as a function of the homologous temperature—the operative temperature divided by the melting temperature ( $T/T_m$ )—and normalized tensile stress—the applied largest principal stress divided by the elastic modulus ( $\sigma_1/E$ ). Of relevance here is load case (ii) discussed above, in which we have:  $T/T_m = 373/1356 \approx 0.27$  and  $\sigma_1/E = 150 \text{ MPa}/108 \text{ GPa} \approx 1.4 \times 10^{-3}$ . A representative view of the creep void growth mechanisms that can be expected to be operative at grain boundaries in copper for load case (ii) can be found in Figure 13 in their paper. This figure suggests that void growth would be *controlled by surface diffusion with a weak coupling to and contribution from power-law creep*. Ahead of a notch or a blunted crack-tip, where stress triaxiality would be elevated and the principal stress would be higher, a stronger contribution from power-law creep to cavity growth is anticipated. It should be noted that there is great uncertainty regarding the set of material parameters used for this figure. For instance, a pre-existing homogeneous distribution of cavities on grain boundaries with relative void area  $f_h = 0.01$  is assumed. With an assumed spacing between cavities of 24 microns, the diameter of a cavity becomes 2.4 microns ( $f_h = ([\text{cavity diameter}]/[\text{cavity spacing}])^2$ ). This is likely to be much larger than can be expected in the copper to be used for the canisters. The figure also contains iso-contours of the damage-rate,  $df_h/dt$  (change in relative void area at grain boundaries per unit time). These iso-contours do not extend to the point in the void growth maps representing load case (ii) (the ratio  $T/T_m$  is too low), but by a simple extrapolation it appears that a predicted damage rate of approximately  $10^{-14}$  (1/s) would be relevant. As an example 31.8 thousand years correspond to  $10^{12}$  s. In addition, the time required to nucleate the cavities is not considered in the figure. Hence, it is unlikely that fracture would occur over this time period based on the information in Figure 13 in Cocks and Ashby (1982). Additionally, it is important to note that the stresses that result in the canister under load case (ii) are primarily compressive with a stress triaxiality that is negative. Growth of cavities and voids under inelastic deformation generally requires a stress triaxiality that is positive otherwise cavities tend to decrease in size and close up, cf. Benzerga and Leblond (2010).

Models for matter transport by surface diffusion applicable to cavity growth on grain boundaries have been developed by Chuang and Rice (1973), Chuang et al. (1973) and Needleman and Rice (1980). Based on their analysis, Cocks and Ashby (1982) provide an approximate analysis that leads to a relatively simple model for cavity growth controlled by surface diffusion. If cavity growth was also influenced by power-law creep, Cocks and Ashby (1982) conclude that diffusion controls the early part of growth, whereas power-law creep takes over as the cavities become larger and the net section stress rises. Moreover, the coupling between these two mechanisms may, for most practical purposes, be adequate to assume that the coupled rate for cavity growth is the sum of rates from each mechanism treated individually. Cocks and Ashby (1982) then propose that the growth rate of the relative cavity (or void) area on grain boundaries,  $f_h$ , normalized by the reference strain rate,  $\dot{\epsilon}_0$ , may be given as

$$\frac{1}{\dot{\epsilon}_0} \frac{df_h}{dt} = \frac{\psi_0 \sqrt{f_h}}{(1-f_h)^3} \left( \frac{\sigma_1}{\sigma_0} \right)^3 + \beta \left[ \frac{1}{(1-f_h)^n} - (1-f_h) \right] \left( \frac{\sigma_e}{\sigma_0} \right)^n, \quad \text{Equation 2-6}$$

where

$$\psi_0 = \frac{1}{\sqrt{2}} \frac{D_s \delta_s \Omega}{k T l \gamma_s^2} \frac{\sigma_0^3}{\dot{\epsilon}_0}. \quad \text{Equation 2-7}$$

Here, the first term represents the contributions from surface diffusion and the second term represents the contributions from power-law creep. In the above equations,  $\sigma_1$  is the normal stress acting on the (grain boundary) plane of the cavity,  $\sigma_0$  is a reference stress,  $n$  power-law creep exponent,  $\beta$  is a parameter that depends exponentially on the triaxiality of the stress state and decrease for decreasing values of triaxiality and vice versa (equal to about 0.6 in uniaxial tension),  $\sigma_e$  is the von Mises

equivalent stress,  $D_s \delta_s$  is the surface diffusion coefficient times its diffusion thickness,  $\Omega$  is the atomic volume,  $k$  is Boltzmann's constant,  $T$  is the absolute temperature,  $\gamma_s$  is the surface free energy,  $2l$  is the centre-to-centre cavity spacing. The iso-contours of the constant damage-rate,  $df_h/dt$ , shown in Figure 13 in Cocks and Ashby (1982) are calculated from Equations (2-6) and (2-7). Numerical treatment of the analysis surface diffusion is discussed by Pan and Cocks (1995), where a coupled surface and grain-boundary diffusion model is developed to address arbitrary grain-boundary network with pores of arbitrary shape.

The damage process leading to intergranular creep fracture is initiated by nucleation of cavities at grain boundaries. There are several possible mechanisms that may cause cavity nucleation e.g., vacancy accumulation, grain boundary sliding and dislocation pile-ups. Grain boundary sliding has been observed to occur in the Cu-OFP of interest here (Sandström et al. 2016, Ayensu and Langdon 1996), and nucleation of cavities may then occur at triple points due to build-up of stress concentrations. For further discussions on nucleation, see Kassner and Hayes (2003) and the references therein.

Grain boundary sliding is of importance not only for cavity nucleation, but also for diffusional cavity growth. It has the effect of causing stress concentration and raising the stress triaxiality locally at some grain boundaries. Cocks and Ashby (1982) argue that sliding is a necessity for diffusional cavity growth. Argon et al. (1992) developed an advanced micromechanically based model to address the effects of grain boundary sliding, in which the evolution of grain boundary facet cracks is the major form of damage that leads to material failure. Onck and van der Giessen (1998a, b) developed a microstructurally based numerical model to study intergranular creep fracture accounting for the different size scales involved i.e., the growth of a single cavity along a grain boundary towards the development of micro-cracks on the order of grain size and their interaction with a macro-crack. Within the framework of continuum damage, Hayhurst et al. (1984) developed models suitable for finite element analysis of creep crack growth. They investigate centre- and edge cracked panels of several materials including copper at 250 °C, and observe that the incipient increment of growth was at an angle larger than 45 degrees relative to the initial crack plane due to excessive blunting prior to the onset of creep crack growth. Moreover, creep growth in copper did not show any sensitivity to specimen geometry. These observations are relevant to the location of the incipient crack growth increment observed in the current study.

A crucial step in modelling creep fracture with parameters obtained in creep tests of a relatively short duration is to provide accurate long term creep fracture estimates. Based on the mechanistic models proposed by Cocks and Ashby (1982) the normalized time to fracture (normalized by a reference strain rate) can be written as a function of the initial damage (area fraction of cavities on grain boundaries), material parameters and applied stress. This is similar to the relation discussed in Section 2.5. In recognition of the uncertainty of model parameters some authors restrict extrapolation to three times the longest validated test available, cf. Wilshire (2003).

Cocks and Ashby (1982) also compare the mechanistic models presented in their paper to continuum damage models proposed by Kachanov (1958), Rabotnov (1969) and Leckie and Hayhurst (1977). They conclude that for large values of damage, quantified by the relative void area at grain boundaries ( $f_h$ ), both modelling concepts would yield the same response. However, at low values of initial damage, typical for diffusional growth of cavities as would be the case for the copper canisters, there is a notable difference between the two concepts. The mechanistic type of models would predict a much slower growth rate of damage for such cases.

## 2.7 Summary of fracture models for Cu-OFP

Two load cases of importance for the integrity of the copper canister were identified. A literature survey was performed to identify the possible modes of failure for these two load cases, which suggest the following:

The mode of failure in load case (i)—slow to high rate of loading at room temperature and below—is expected to be ductile fracture. Based on the literature and the tests performed by the commission of SKB, it is concluded that ductility or strain to failure is expected to be very high in Cu-OFP.

Loading at increased strain rates, on the order that may come into play during a rock shear movement, can be expected to have minimal influence on the ductility of Cu-OFP. There are well established and verified models for the analysis of ductile failure and fracture in copper described in the literature.

In load case (ii)—constant-pressure loading at approximately 100 °C—the possible mechanisms that may lead to failure are less clear. If the stress levels were sufficiently high the canister would again fail by ductile failure. However, the load levels foreseen for this case will not be sufficiently high to promote ductile failure. The question then arises whether the copper canister can fail by creep fracture or not i.e., by transgranular or intergranular creep fracture. The latter would require that the overall strain would be excessive at failure, which can be excluded due to the kinematic constraints acting on the copper canister (caused by the insert of nodular cast iron). Thus, the remaining question is whether intergranular creep fracture can occur. The literature survey suggests that a possible mechanism for progression of creep damage along grain boundaries would be cavity growth controlled by surface diffusion with an influence (possibly weak) of power-law creep. However, for the relatively low homologous temperature to which the copper is exposed, combined with the kinematical constraint to which copper canister is subjected, no support was found in the literature indicating that intergranular fracture would be likely to occur.

### 3 Background data—previous testing

The following is a brief presentation of the background data, methods used and general CCG testing with CT specimens. Few studies of CCG are available for Cu-OFP, and in this work, four main studies are represented: Seitisleam and Henderson (1995), Andersson (2005) and Wu et al. (2011, 2013).

The CT specimen type used for all tests except in Seitisleam and Henderson (1995) was CT-50, where -50 stand for the size. The dimensions and appearance are given in Figure 3-1 and Figure 3-2. In Seitisleam and Henderson (1995), a CT-25 specimen was used. Side grooves were used for some of the specimens.

The crack tip opening or load line displacement (LLD) is measured using a beak type extensometer; see Figure 3-2. The stress state around the crack tip changes with the size of specimen owing to the larger constraint in larger specimens.

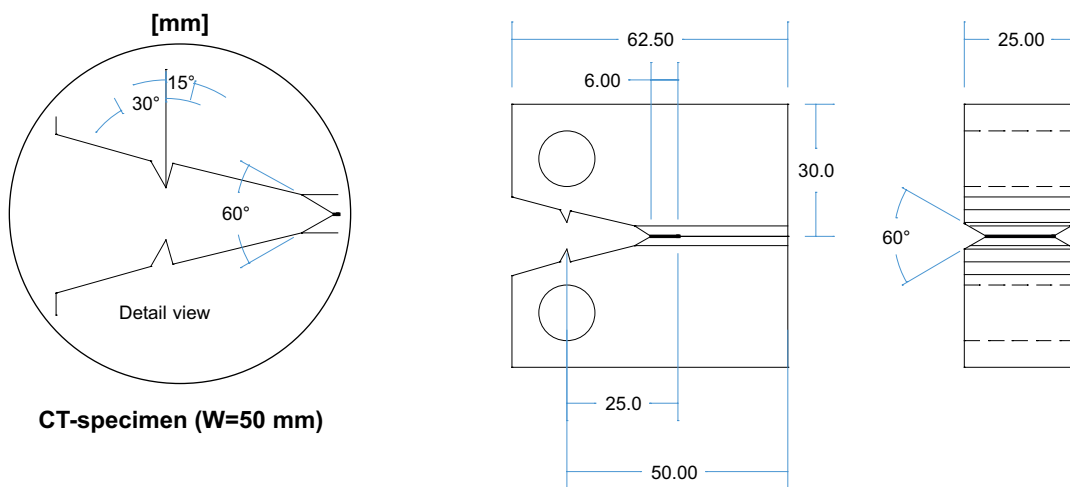


**Figure 3-1.** Dimensions for CT-50 compact tension specimen with side grooves.

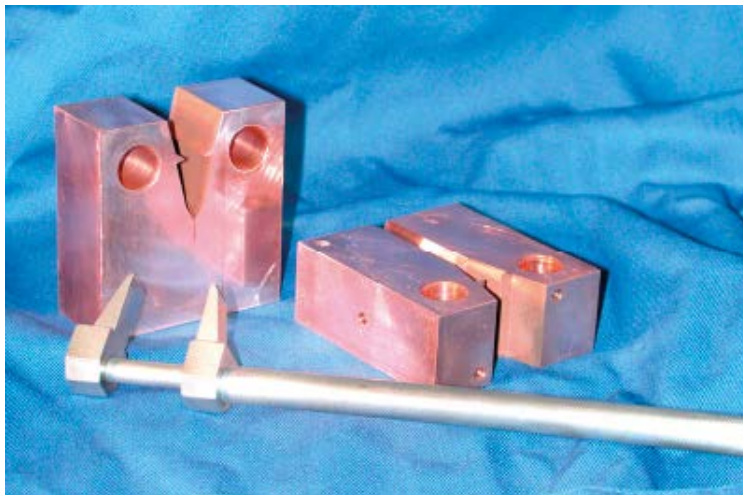


**Figure 3-2.** CT specimens. The instrument in the foreground is a beak type crack tip opening displacement extensometer gage.

The crack extension was measured in the present cases by the potential drop (PD) method; however, this was not successful. Potential drop measurements work such that an electrical current is led through the specimen across the crack propagation plane. The potential drop across the same propagation plane is then measured, and when the crack grows, the cross sections area decreases and the potential increases. The method can successfully be used on, e.g., steels and nickel-based superalloys. Because of the good electrical conductivity of Cu-OFP the PD method did not show to constitute a practicable method. No distinct signal was received and no crack extension was measured; also see Figure 3-3.

The load applied to the CT specimens is based on the stress–rupture time relationship obtained from plain uniaxial creep specimens and is calculated using the reference stress concept (Miller 1988). A common way of defining the reference stress ( $\sigma_{ref}$ ) for a CT specimen is

$$\sigma_{ref} = \frac{P}{mB_nW} \quad \text{Equation 3-1}$$

where  $P$  is the load applied to the specimen, and  $B_n$  is the net thickness of the specimen with side grooves. The coefficient  $m$  can be evaluated according to the von Mises criterion as plane stress or plane strain. The plane stress expression is

$$m = -\left(1 + \gamma\left(\frac{a}{W}\right)\right) + \sqrt{\left(1 + \gamma\right)\left(\left(\gamma\left(\frac{a}{W}\right)\right)^2 + 1\right)} \quad \text{Equation 3-2}$$

$$\gamma = \frac{2}{\sqrt{3}} \quad \text{Equation 3-3}$$

and the plane strain expression is

$$m = \frac{2}{\sqrt{3}} \left[ -\left(1 + \gamma\left(\frac{a}{W}\right)\right) + \sqrt{\left(1 + \gamma\right)\left(\left(\gamma\left(\frac{a}{W}\right)\right)^2 + 1\right)} \right] \quad \text{Equation 3-4}$$

$$\gamma = 1.702 \quad \text{Equation 3-5}$$

where  $a$  is the crack depth calculated from the load line, and  $W$  is the length from the centre of the load pin holes to the back of the specimen. It should be emphasized that the equation for the reference stress is derived from limit load analysis. Thus,  $\sigma_{ref}$  should be interpreted as the yield stress in an elastic, ideal plastic material, and the load  $P$  on the right-hand side is the corresponding limit load. Therefore, the reference stress would, for instance, change (increase) as the crack extends ( $a$  increases) under constant load  $P$ . The ratio between the reference stress and the initial yield stress, 60 to 70 MPa in the temperature interval of interest here, then gives direct information about the level of plastic deformation to which a specimen has been subjected prior to the creep test. Furthermore, experience has shown that the initial reference stress for CT specimens can be related to the uniaxial stress for a plain creep specimen. A way of visualizing this phenomenon is to view the material in front of the crack tip as comprising an infinite number of small uniaxial creep test rods, Figure 3-4.

The time taken for the first rod to rupture owing to creep can be roughly compared to the time necessary for a uniaxial specimen made from the same material to rupture at the stress prevailing at the crack tip.

It should be noted that the reference stress is an analytic expression that presumes small deformations. The extensive deformations experienced in the CT Cu-OFP specimens, Figure 3-5, will inevitably alter the outcome. This means that the real resulting stress probably deviates from the level predicted by Miller (1988); however, there is no better alternative at hand without carrying out a considerable finite element analysis.

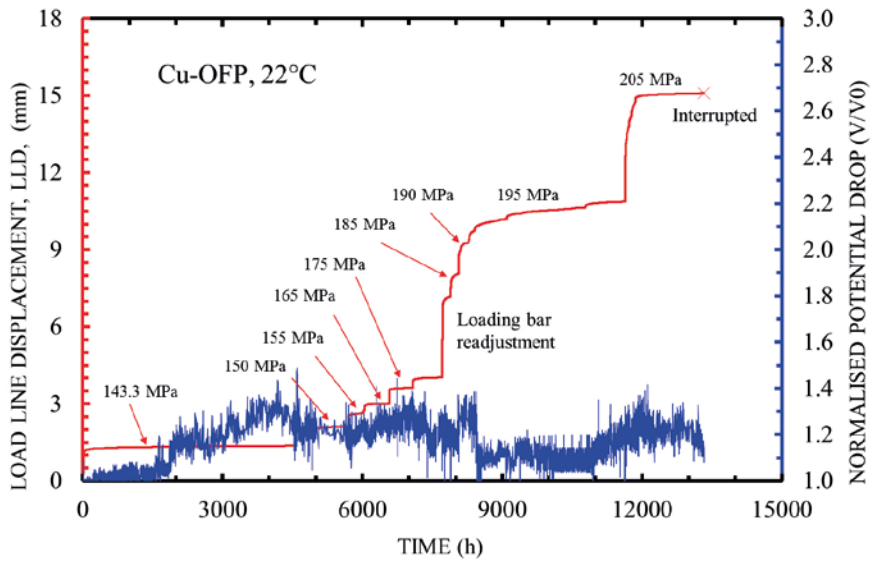


**Figure 3-3.** Load line displacement (red line) and normalized potential drop (blue line) as a function of time for the CCG tests at 22 °C.

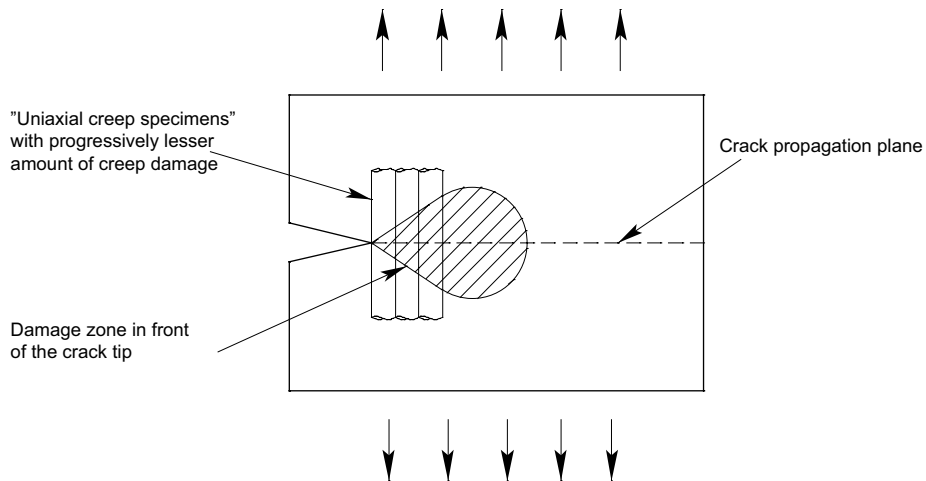


**Figure 3-4.** The idealized steady state creep crack growth process in which the material in front of the crack tip is divided into an infinite number of uniaxial creep specimens.

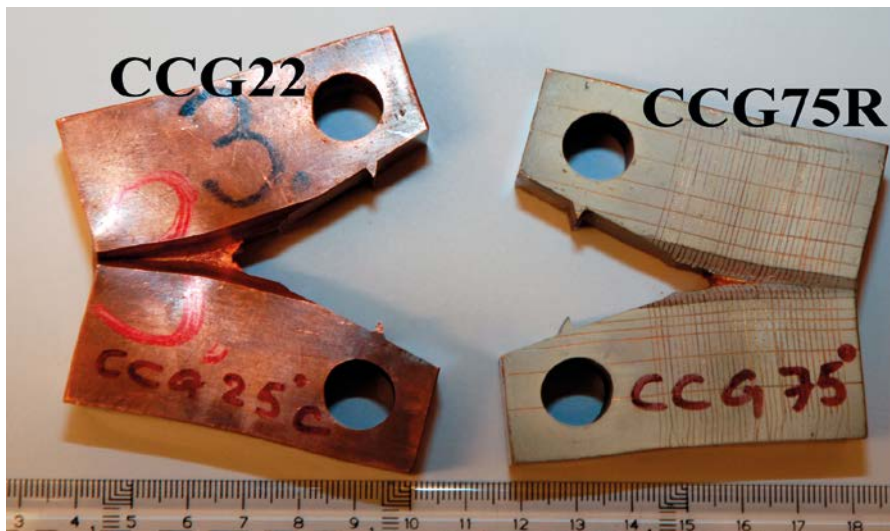


**Figure 3-5.** Extensive deformation of Cu-OFP creep crack growth on CT specimens.







**Figure 4-2.** One end of a failed cylindrical Cu OFP creep specimen; note the extreme level of necking. The specimen is split alongside, thus the burrs at the edges.

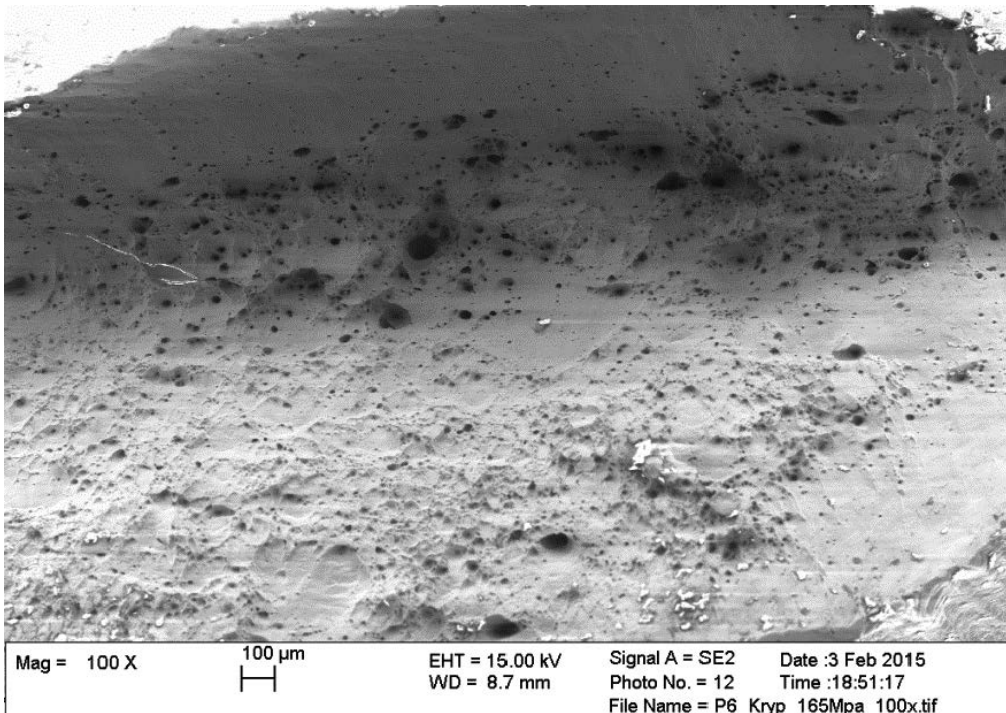


**Figure 4-3.** Non-brittle creep rupture in a plain cylindrical copper uniaxial creep specimen. The picture shows the fracture surface.

At higher magnification, Figure 4-4, it can be seen that all cavities are lengthened in the main creep direction (perpendicular to the paper). Almost all dimples seem to have originated in a small cavity, and during elongation (i.e., creep), the inside walls of the cavities have been stretched, resulting in relatively smooth surfaces with a texture from shear flow that looks like irregular stripes. Wakes in shape of dragging marks from micro-cavities can also be seen at the strained dimple walls.

When viewing the creep specimen from a length section (Figure 4-5), it can be seen that the rupture shows typical and clear signs of being non-brittle. There is pronounced necking, and the final rupture has very clear shear lips. When viewing the final rupture more closely (Figure 4-6), surface flaws and flaw-like “delamination” areas can be found just under the surface. Spots where shrinkage has occurred, i.e., cavities, have been formed and/or enlarged. The cavities can be, e.g., creep cavities at grain boundaries and the origin of the craters that was observed at the fracture surface of the specimen.

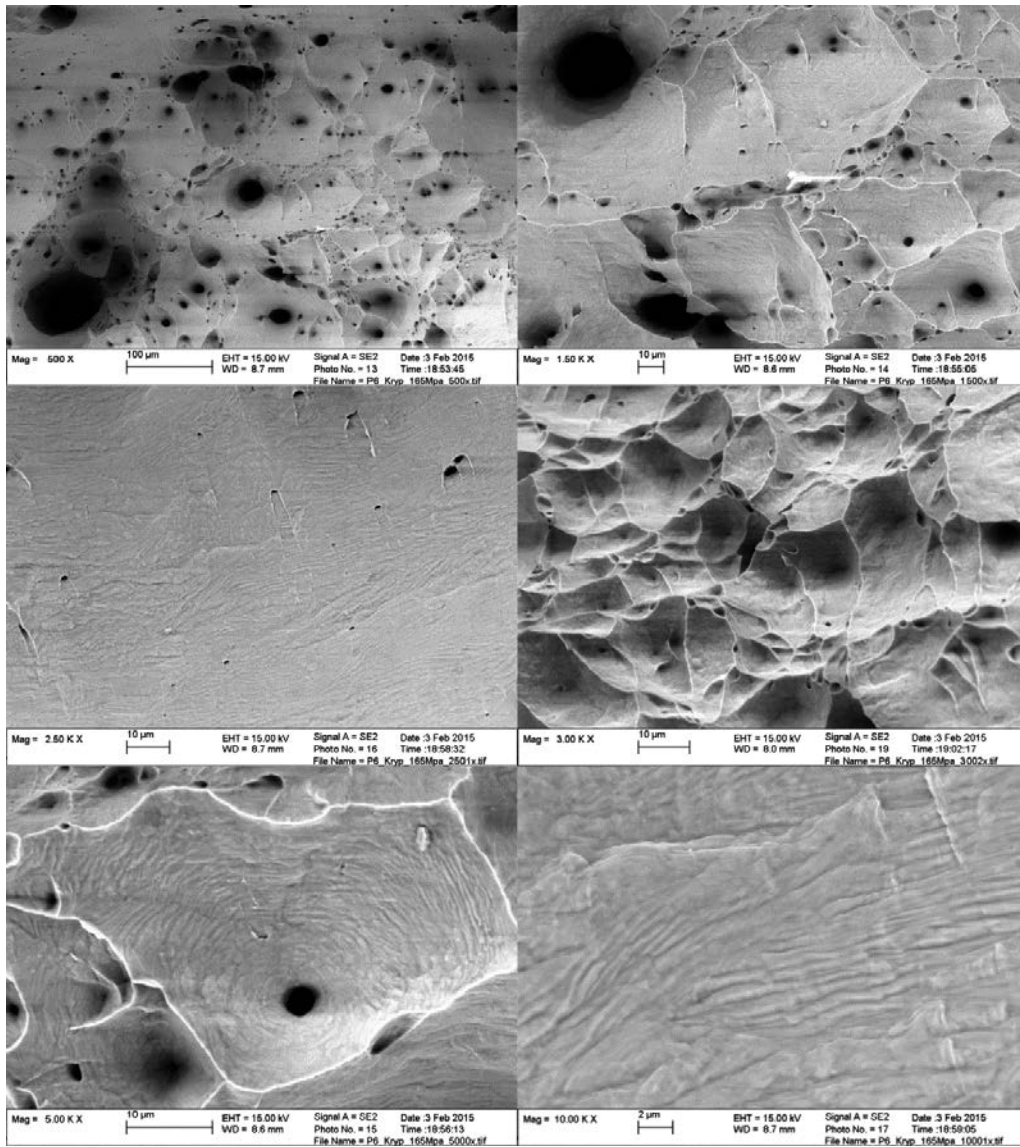


*Figure 4-4. Close-up of different zones and magnifications of the creep rupture in Figure 4-3.*

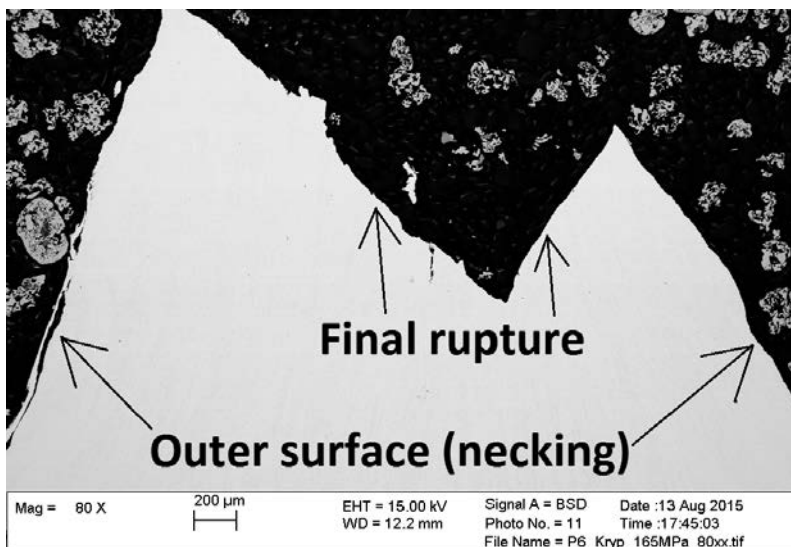


*Figure 4-5. Length section through the 10 mm round specimen. The direction of force was vertical. Note the extensive necking and the shear lips indicating a tough fracture.*

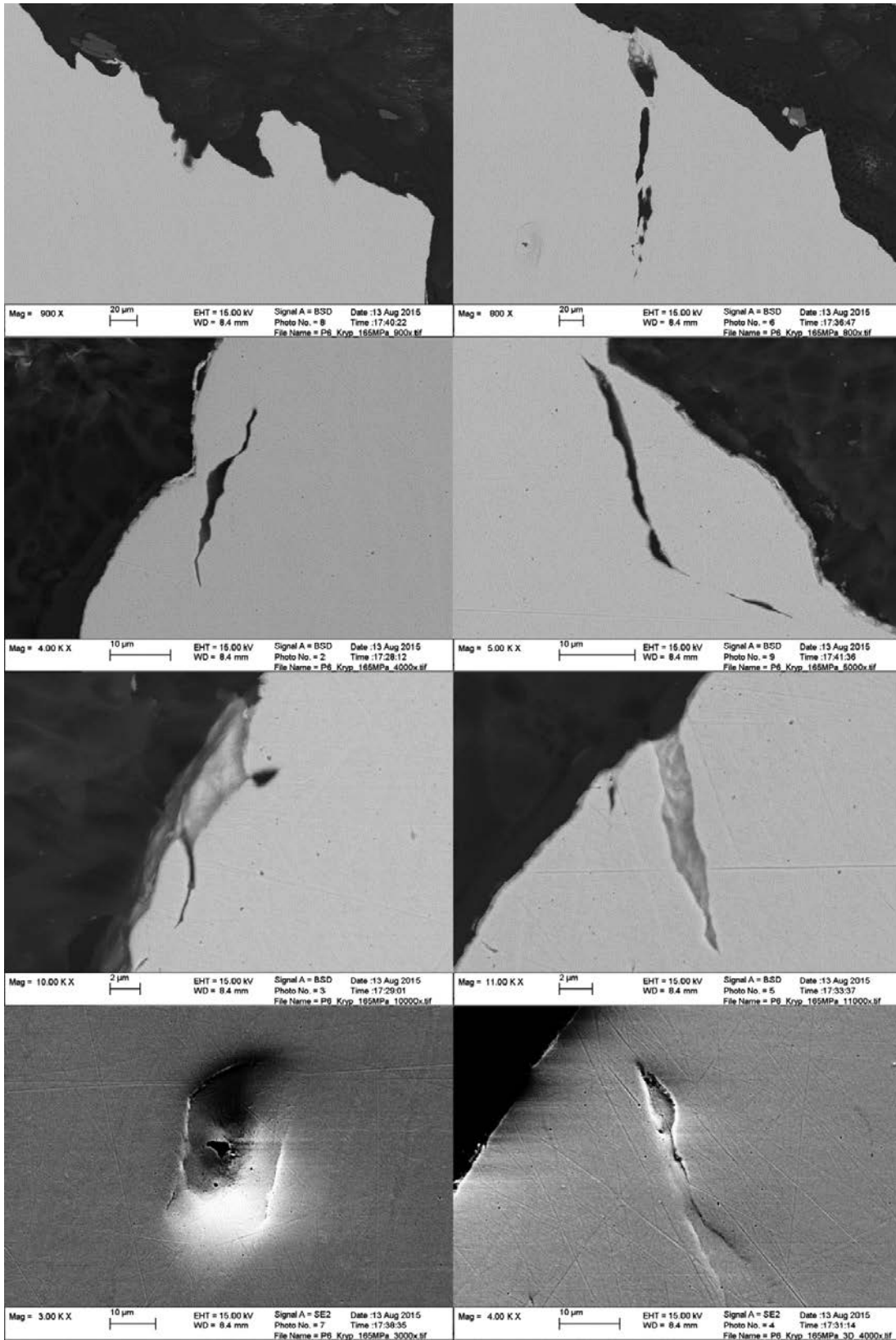


**Figure 4-6.** Flaws and different types of cavities from the fracture surface or near the fracture surface of the regular uniaxial creep specimen.

### 4.3 Cut-up views from CCG CT specimens

The massive amount of strain experienced in the CT specimens at the present force levels suggests that triaxiality prevails at the notch root, i.e. where the crack is supposed to form. Therefore, it could be expected that creep damage would appear in almost any plane at this location, not only in the main stress direction, but also, e.g., in the transverse direction (there is one exception, 45° slip planes formed above the plastic strain limit). To investigate this phenomenon, the area adjacent to the notch of the specimens was cut in the length direction (A–A), the perpendicular direction (B–B) and the transverse direction (C–C).

In Figure 4-7, the present cut-up planes are illustrated. Note that for views B–B and C–C, surfaces not emanating from fracture but from the notch area can be found, both from the main notch and from the side grooves. Those surfaces are, however, highly strained near and at the notch bottom; thus, they are sometimes a bit difficult to distinguish from the actual crack surfaces within the fracture area.

In Table 4-1 the test data for the examined CT specimens is presented. The specimen is designated with a generic name and test conditions from respectively test campaign. There is no specific order between them.

**Table 4-1. Data for the examined CT specimens. Note that specimens GGG125-1 and CCG125-2 is referenced twice.**

Specimen no	Designation	View	$\sigma_{ref}$ [MPa]	Temp. [°C]	Test Interruption [h]
1	CCG100	A–A	185	100	2925
2	CCG125-1	A–A	165	125	2256
3	CCG175	A–A	115	175	12286
4	CCG125-1	A–A	165	125	2256
5	CCG125-2	A–A	165	125	1577
6	CCG75A	C–C	165	75	8925
7	CCG125-2	B–B	165	125	1577

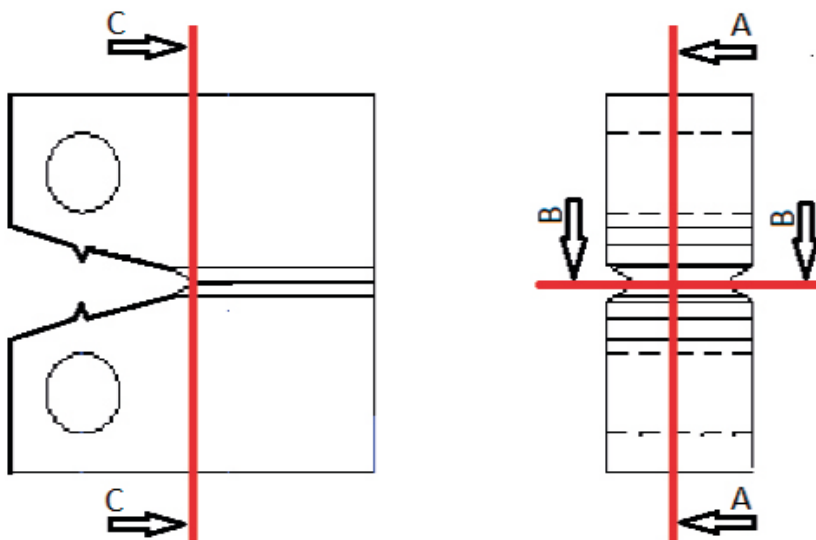


**Figure 4-7.** Cut-up planes for CT specimens with viewing of planes A–A, B–B and C–C. Cut C–C is in front of notch bottom, thus giving a view at notch bottom.

#### 4.3.1 View A–A from specimen no 1 ( $T = 100\text{ }^{\circ}\text{C}$ , $\sigma_{\text{ref}} = 185\text{ MPa}$ )

The specimen is cut in the A–A viewing plane. Figure 4-8 shows the notch root and various magnifications of the innermost notch tip. It can be seen that numerous cavities have been formed in the bulk near the notch surface. This indicates that the material at the notch root experiences a load high enough to cause creep. The crack-like cavity (pictures on the right) is located under the surface of the notch tip. Noting the width of the cavity, it has most probably emanated from a weak spot in the material (e.g. a grain boundary) about 15–20  $\mu\text{m}$  under the surface. After that, the narrow ligament between the cavity and the surface has collapsed, and a surface breaking crack has formed. This has happened without any noticeable blunting, note the in width between cavity and crack. It does not grow perpendicular to the force direction but along the slip line formation occurring at a blunted crack, which is consistent with the theory on slip lines of blunted cracks (Rice and Tracy 1969). The blunted inner end of the cavity still indicates tough behaviour.

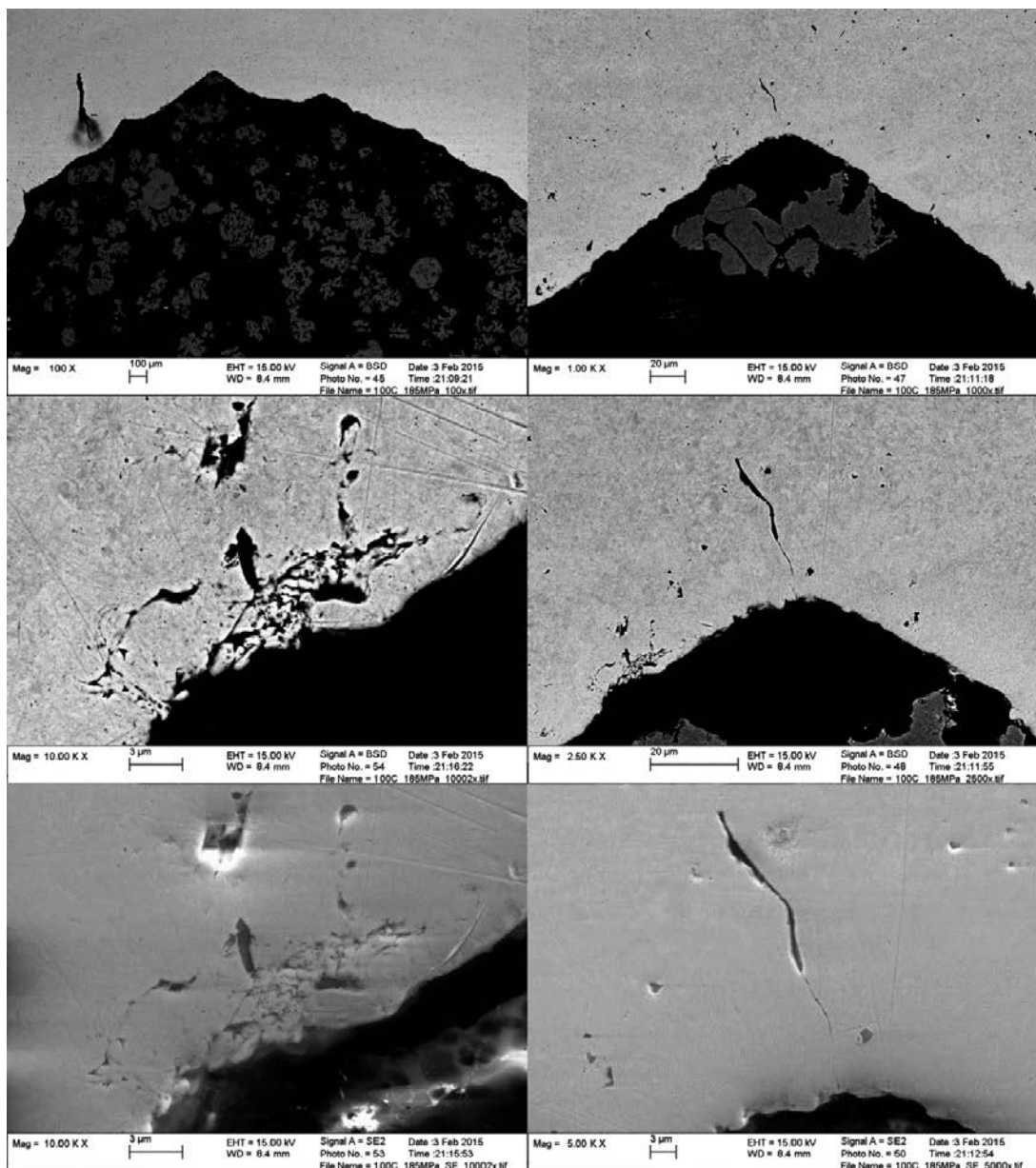


**Figure 4-8.** Specimen no 1, tested at 100 °C and reference stress 185 MPa with notch root appearance. The force direction was horizontal.

#### 4.3.2 View A–A from specimen no 2 ( $T = 125\text{ }^{\circ}\text{C}$ , $\sigma_{\text{ref}} = 165\text{ MPa}$ )

The cross view of this specimen (Figure 4-9) shows a similar appearance to the former  $100\text{ }^{\circ}\text{C}$  specimen. At the notch root, a jagged edge is noticed, which is consistent with slip line theory (Rice and Tracy 1969). Larger dents or small flaws can be seen at irregular locations, probably emanating at the location of slip line establishment. All outlines that have been found in this specimen were blunted, indicating that cracks initiated at the surface became blunted under further loading (Hayhurst et al. 1984).

#### 4.3.3 View A–A from specimen no 3 ( $T = 175\text{ }^{\circ}\text{C}$ , $\sigma_{\text{ref}} = 115\text{ MPa}$ )

In Figure 4-10 one can directly see the oxide layer established in the elevated temperature. Disregarding the oxide layer, the appearance is fairly similar to the specimens tested at lower temperatures, yet with a more pronounced tendency to crack initiation without immediate blunting. It should be noted that this temperature is not within the specified range for the final disposal.

#### 4.3.4 View A–A from specimen no 4 ( $T = 125\text{ }^{\circ}\text{C}$ , $\sigma_{\text{ref}} = 165\text{ MPa}$ )

In the cross section of this specimen, Figure 4-11 view A–A, the widespread formation of cavities and shrinkages is clearly seen in the vicinity of the notch root but still under the surface. The cavities are mainly found near the worst stress concentrations, again suggesting that the formation of cavities is driven by constrained stress fields (Rice and Tracy 1969, Kassner and Hayes 2003). It can also be seen that cavities are oriented in different directions and that they have different geometries but with no visible crack formation, see for example Figure 4-12. This indicates the presence of strong triaxiality. Again, only blunted flaws were found.

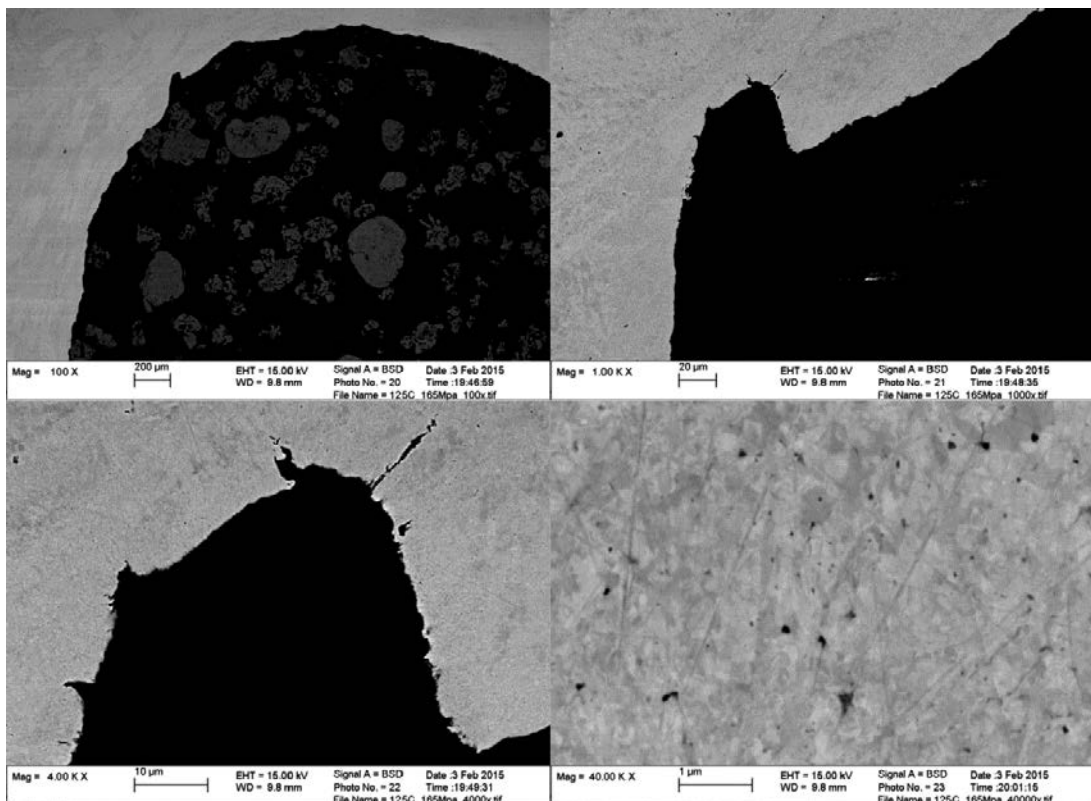


**Figure 4-9.** Specimen no 2, tested at  $125\text{ }^{\circ}\text{C}$  and reference stress  $165\text{ MPa}$ . The force direction was horizontal.

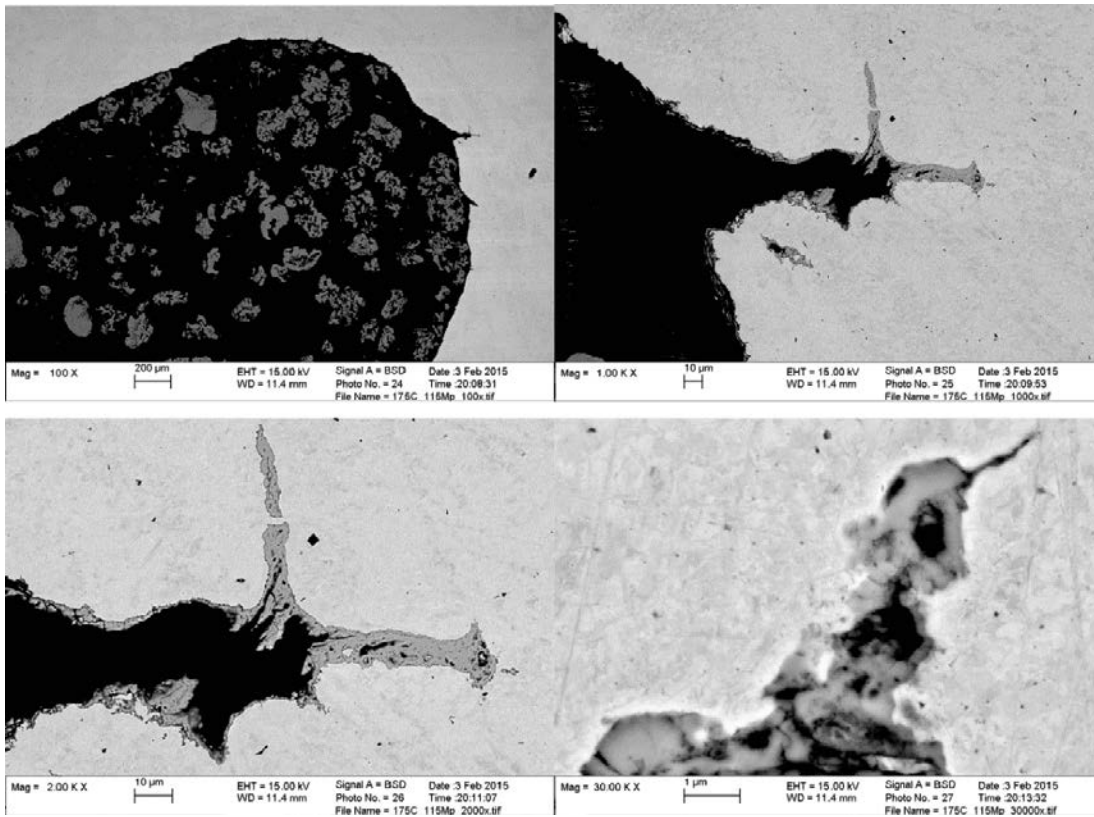


**Figure 4-10.** Specimen no 3, tested at 175 °C. The higher temperature is directly indicated by the oxide layer.

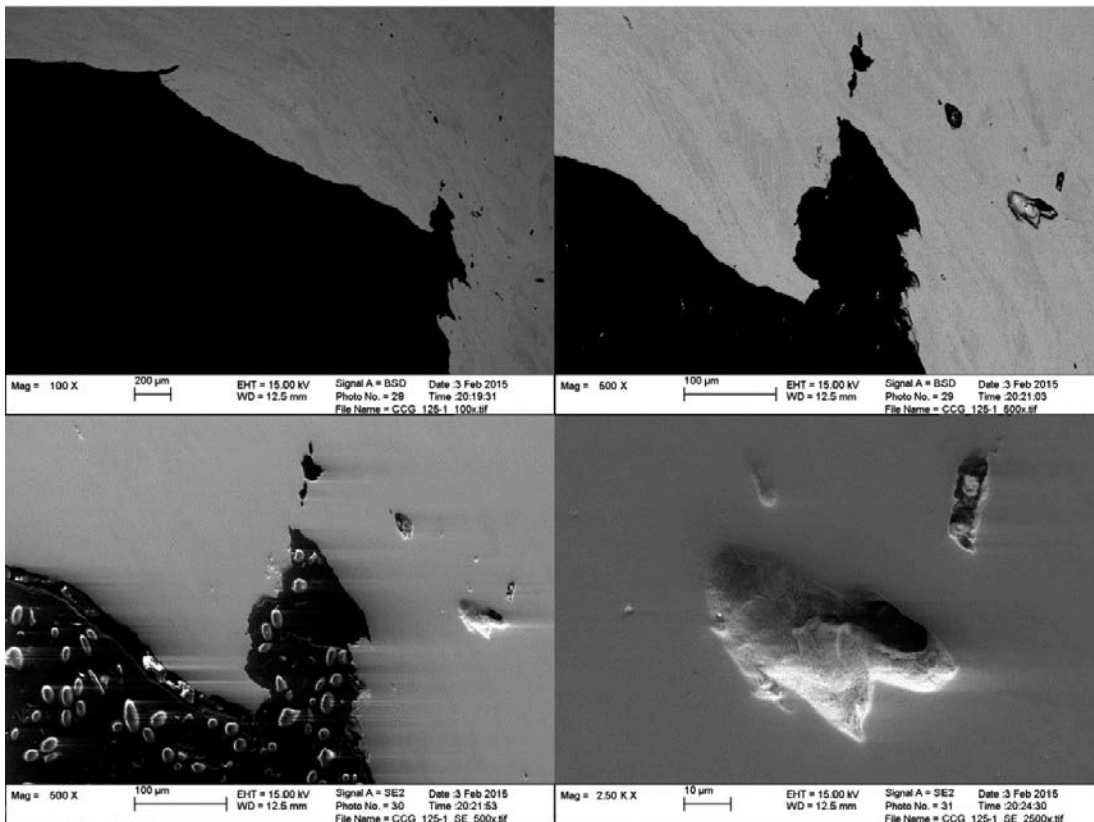


**Figure 4-11.** Specimen no 4. Flaws at the bottom of the notch and cavity formation in the near surroundings.

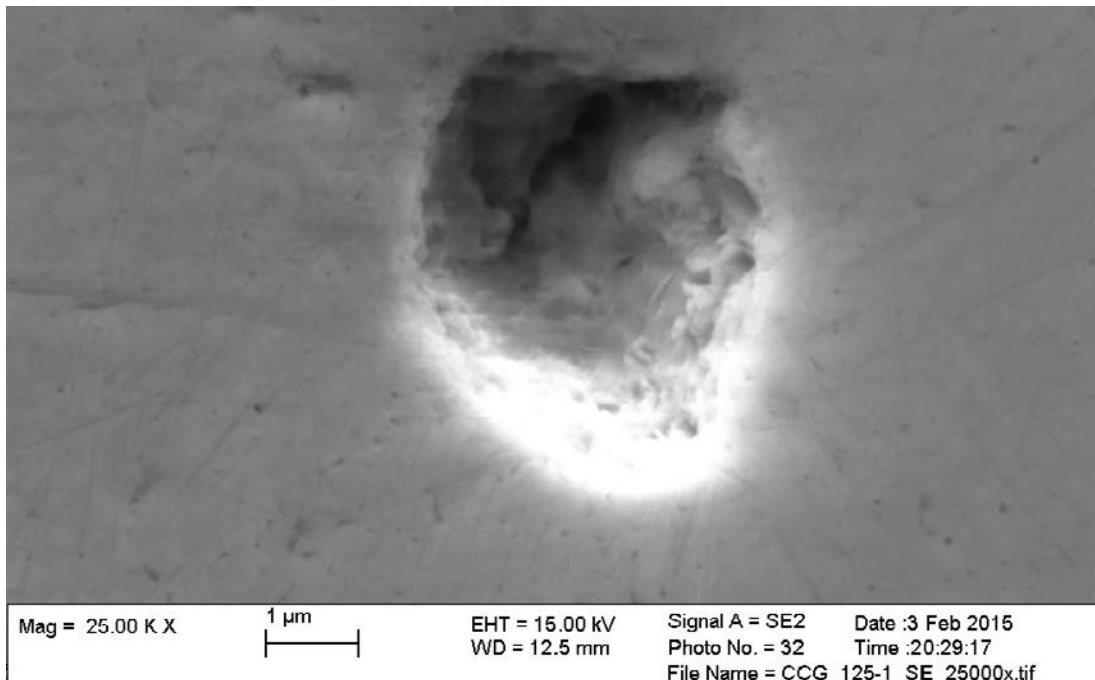


**Figure 4-12.** Close-up of a cavity formation in specimen no 4.

#### 4.3.5 View A–A from specimen no 5 ( $T = 125\text{ °C}$ , $\sigma_{\text{ref}} = 165\text{ MPa}$ )

The macroscopic view, Figure 4-13, shows a cross section similar to the other specimens i.e. a blunted notch bottom showing a jagged contour and a few locations where small flaws have established. Several surface shrinkages and dents appear around the flaws, mainly in the prolonged flaw direction.

At higher magnification (Figure 4-14), it can be concluded that the depressions are small volumes of material that have not followed the rest of the bulk during deformation. In addition, pure cavities appear. The shape and direction of these volumes seem to be stochastic. As seen in Figure 4-15, essentially pure out-of-plane deformation is also represented. As a suggestion, the origin of the formations observed could be creep cavities caused by the present stress state; however, this suggestion cannot be confirmed. It is clear that it is some type of deformation damage, yet it is difficult to determine 3D behaviour from a 2D view.

#### 4.3.6 View C–C from specimen no 6 ( $T = 75\text{ °C}$ , $\sigma_{\text{ref}} = 165\text{ MPa}$ )

These figures (Figure 4-16) are from the bottom of the notch area (view C–C) at the outer surface without any cutting or other treatment; i.e., it is the raw surface at the location where a crack is expected to form. It can be seen that the texture of the surface after yielding is similar to other specimens including the typical “crater holes” after cavities. The force direction was horizontal. The groove in the middle of the figures looks like a crack or a crack initiation, but it is likely a grain boundary. When cutting the specimen perpendicular at exactly this location, no sign of cracks could be identified. From that, it could be assumed that the ridge is a grain boundary that has been open wide during deformation of the specimen, yet not failed. It should also be observed that despite the lack of visible cracks at the perpendicular cut, the validation of a 3D phenomenon from a 2D view is never certain. However, at one location, a cavity oriented along the grain boundary can be seen. This is most likely a creep cavity, i.e. a failure at a limited part of the grain boundary.

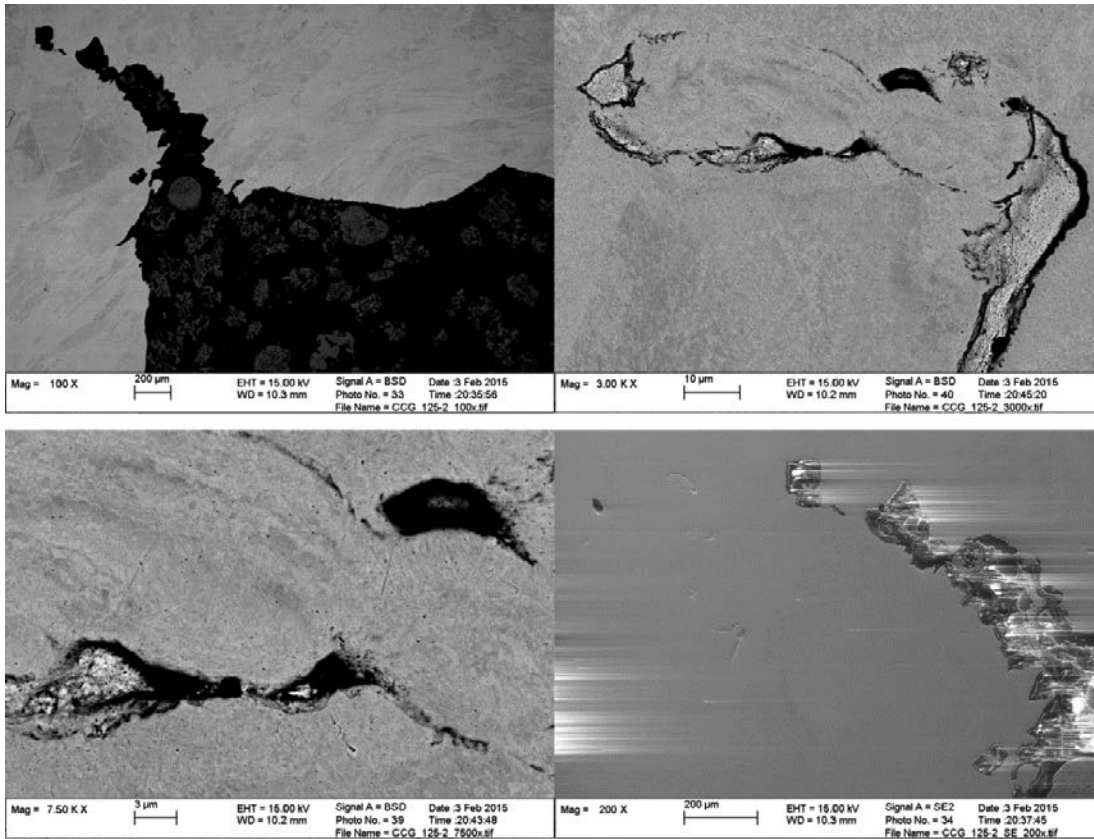


Figure 4-13. Specimen no 5. Wake and deformation damage at notch root (specimen no 4).

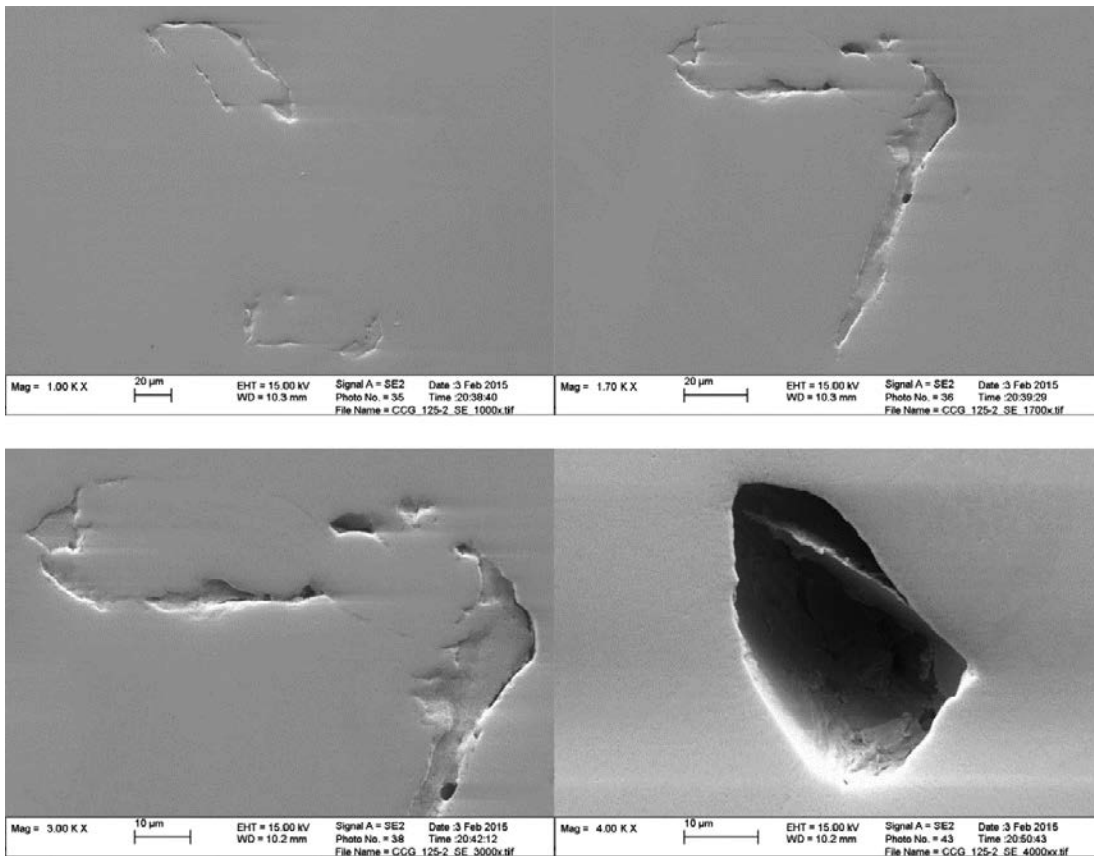
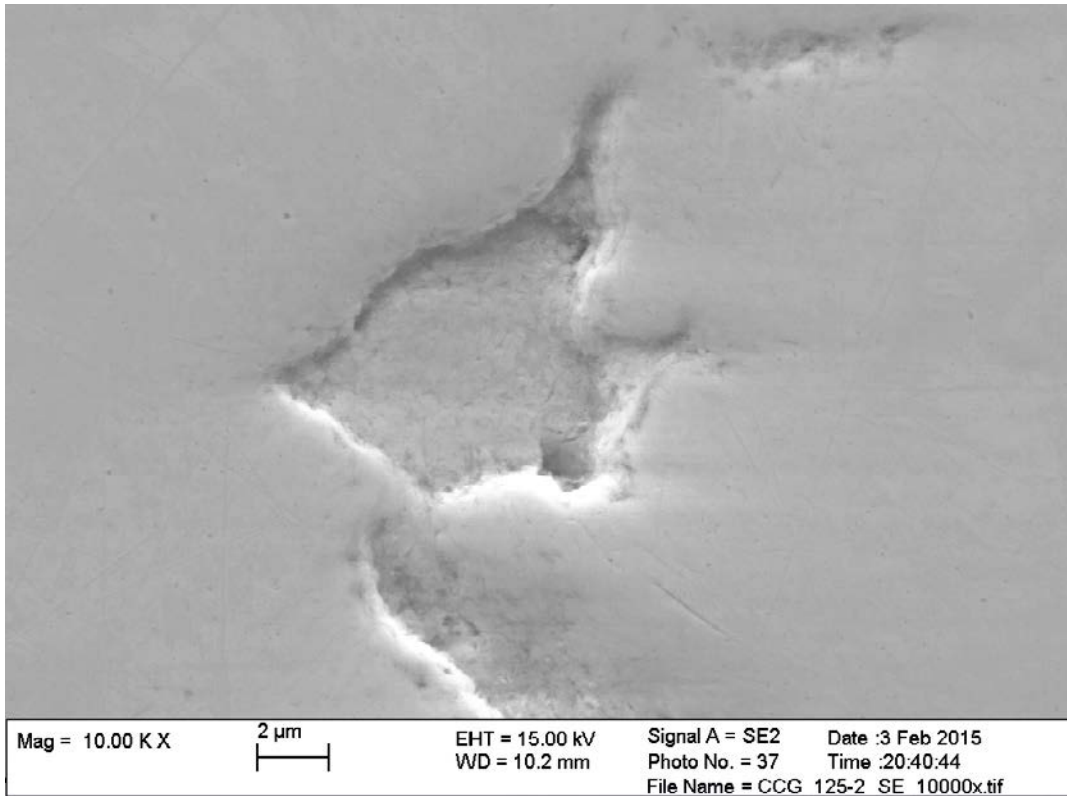


Figure 4-14. Close-up view of the deformation damage in Figure 4-13 (specimen no 5).



**Figure 4-15.** Out-of-plane shrinkage, a probable cut through a cavity near the notch root in specimen no 5 (referring to Figure 4-13).

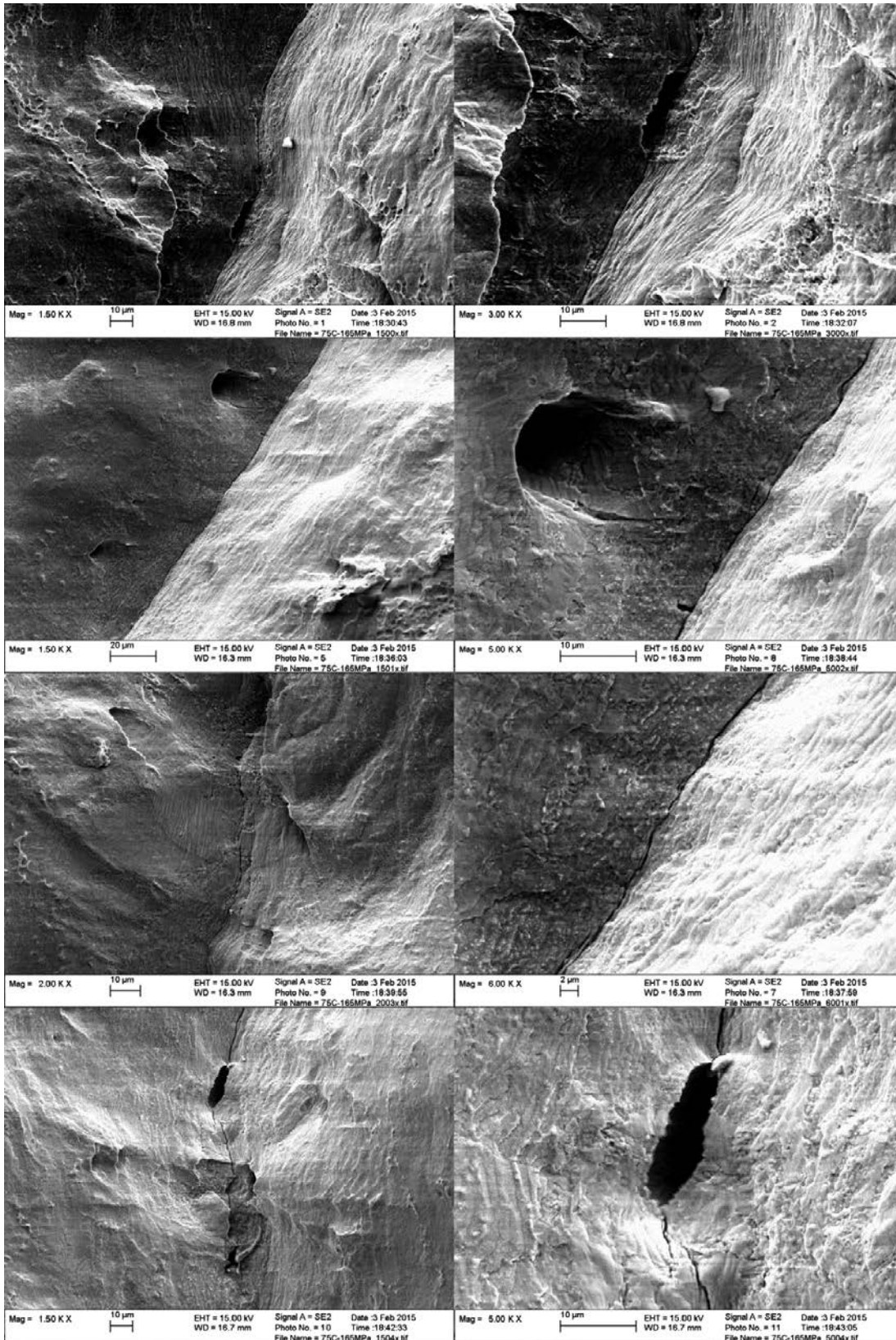


Figure 4-16. Specimen no. 6. Bottom of notch root, view C-C, different locations along the root.

#### 4.3.7 View B–B from specimen no 7 ( $T = 125\text{ °C}$ , $\sigma_{ref} = 165\text{ MPa}$ , separated in halves)

In this CCG CT specimen, a crack-like formation was noticed at the bottom of the notch bottom during test. The specimen is shown in cut-up plane B–B, and the crack propagation area appears.

The first feature to note from Figure 4-17 is that the area of crack propagation has the dimple texture typical of tough fracture. Moreover, the similarity to the area of final fracture is convincing. In the close-up view, Figure 4-18, it can be noted that the fracture surface contains a certain amount of stochastic located wedge-shaped cavities.

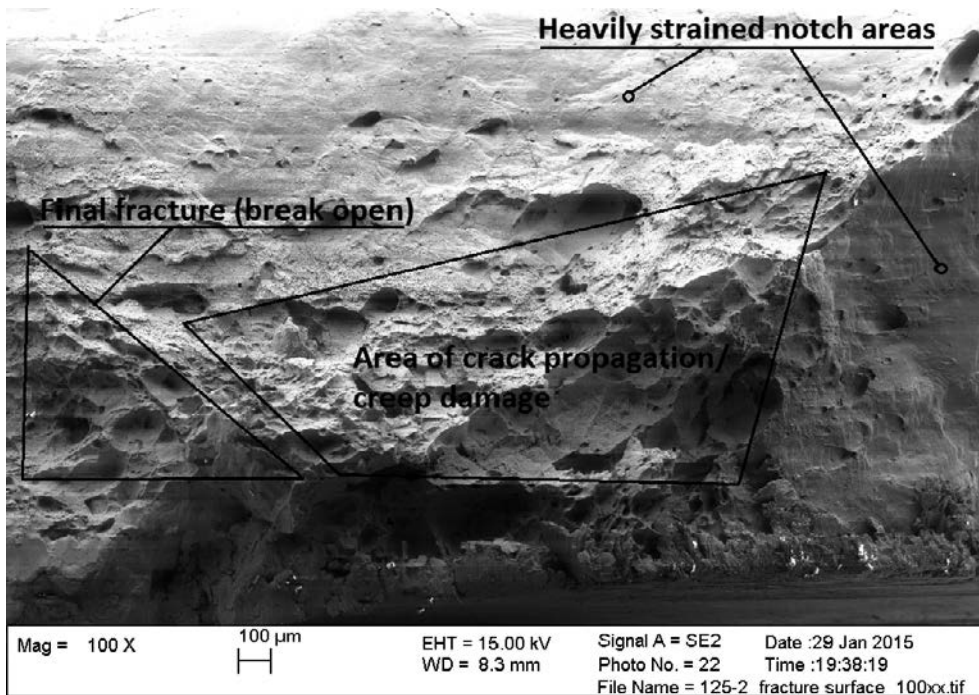


Figure 4-17. Macroscopic view of the different fracture zones in specimen no 7.

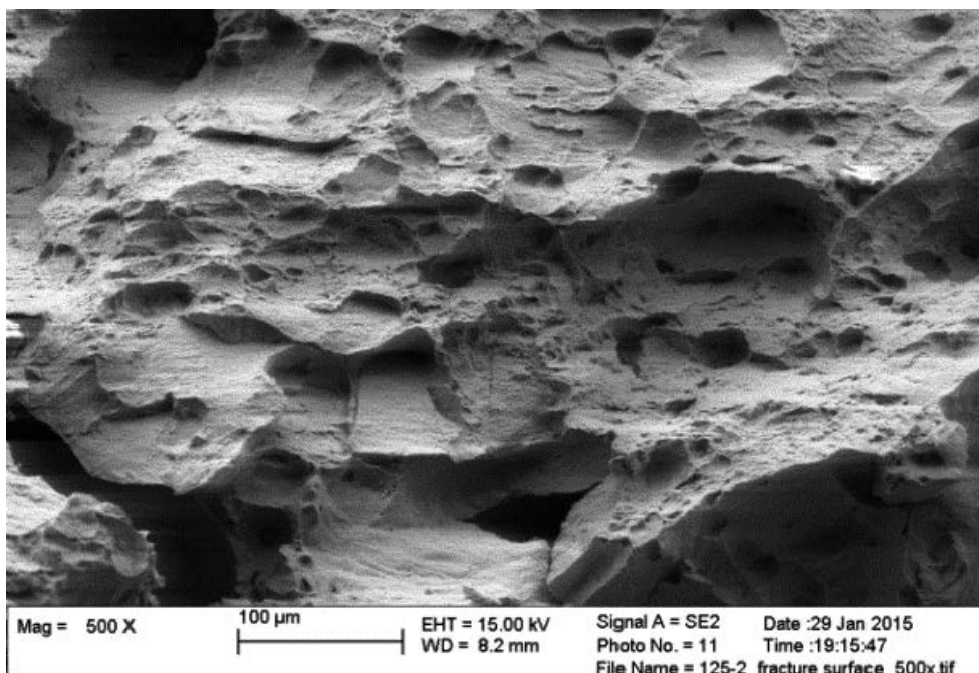


Figure 4-18. Specimen no 7, Magnification of the fracture surface. Note the wedge-shaped cavities.

This is in line with expectations since corresponding randomly oriented cavities have been observed near notch bottoms in all other studied specimens. The random orientations of the cavities strengthen the presumption that the material reaction mainly follows the development dictated by the strong triaxiality during loading of the CT specimen.

The heavily strained material at the notch root next to the fracture (Figure 4-19) exhibits a surface similar to other specimens including the uniaxial creep specimen in Figure 4-1. The surface then shows a smooth transition from the appearance of the strained material to the fracture surface dominated by dimples; see the left part of Figure 4-19.

Also the wakes in shape of dragging marks from micro-cavities can be seen at the strained dimple walls, Figure 4-20.

At higher magnification the fracture surface still have the same characteristics, Figure 4-21. It is in appearance basically similar to the pure fracture surface seen in Figure 4-3.

A look at the fracture surface from the final break-up area (Figure 4-17, Figure 4-22 and Figure 4-23) reveals a texture that is similar to the texture at the propagating fracture (crack propagation) in Figure 4-21. This suggests that the type of fracture is closely related.

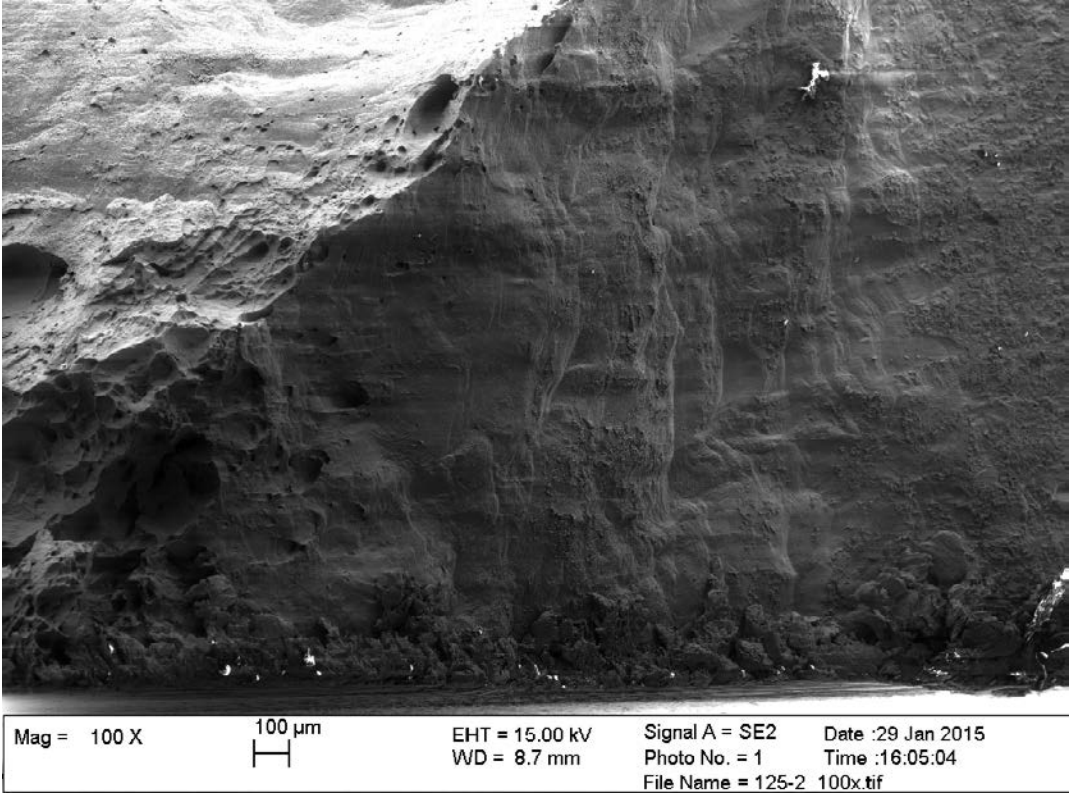


**Figure 4-19.** Specimen no 7. Heavily strained notch area (right and upper) and crack propagation area (down to the left).

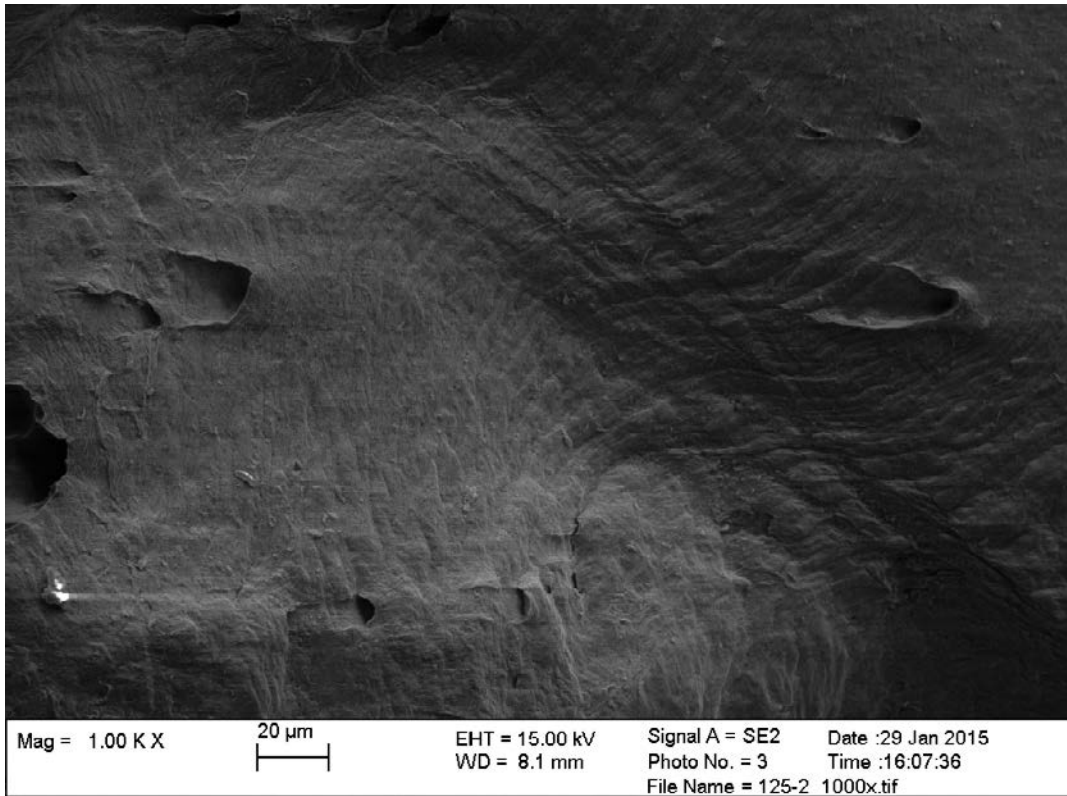


**Figure 4-20.** Specimen no 7. Close-up of the severely strained area at the notch. Note the similarity to strained areas of other specimens.

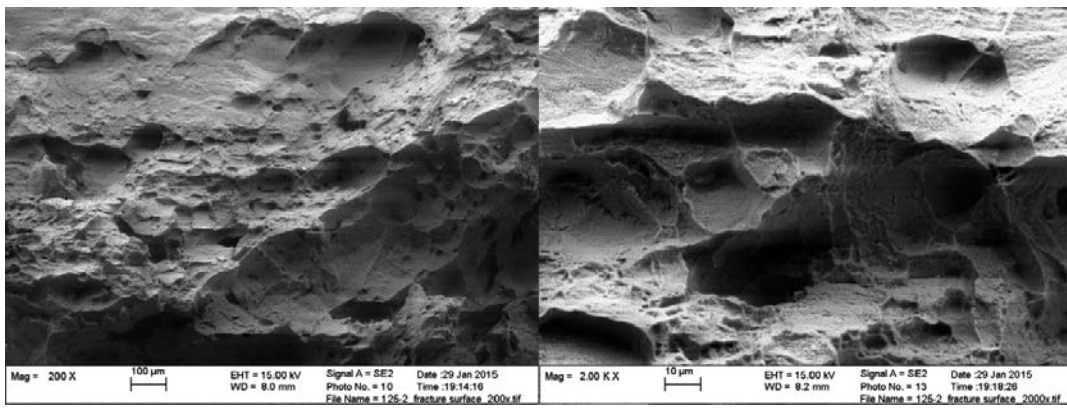


**Figure 4-21.** Specimen no 7. Details of the crack propagation area at different magnifications.

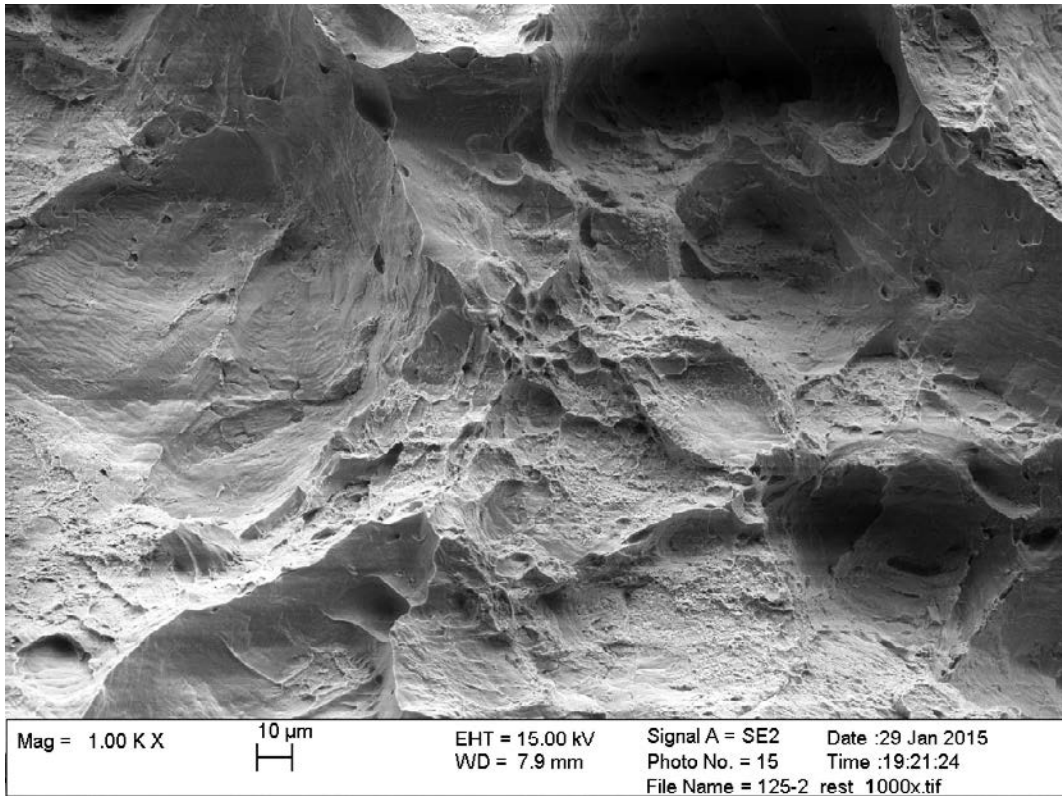


*Figure 4-22. Fracture surface after breaking open (specimen no 7).*

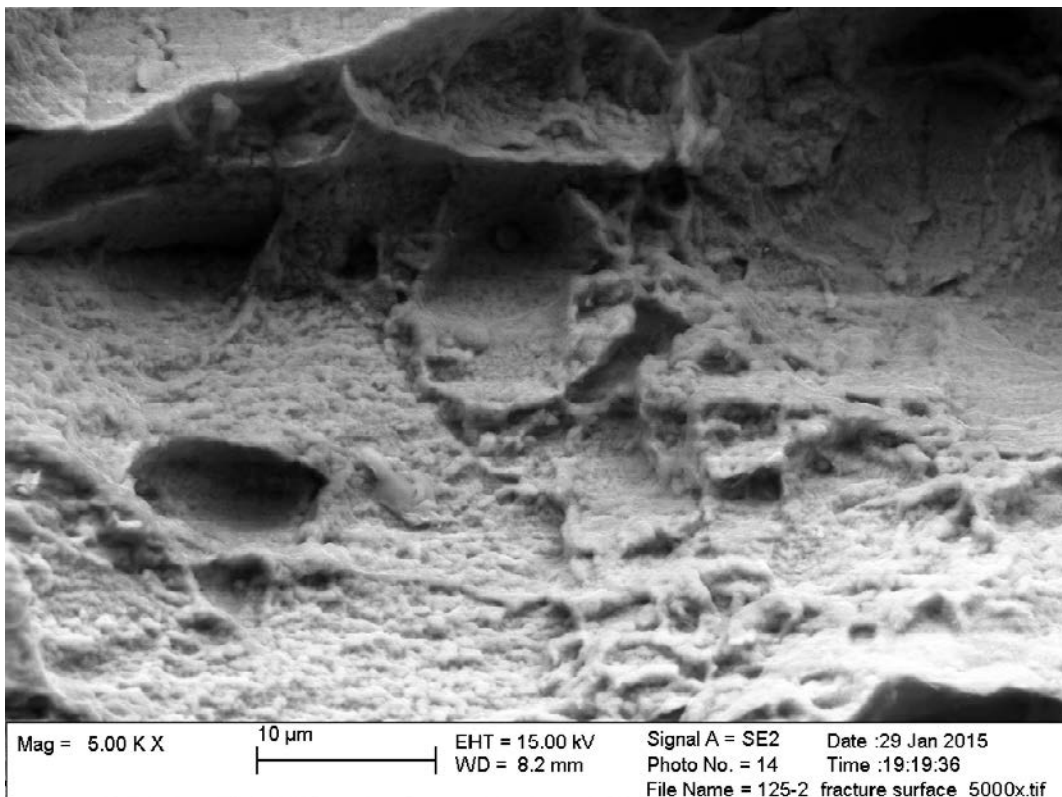


*Figure 4-23. Close-up of Figure 4-22.*

## 5 Discussion and conclusion

Uniaxial and CCG tests on Cu-OFP have been revisited with the purpose of finding evidence of crack growth initiation. The tests were performed in the temperature range 75 °C to 175 °C. The ensuing crack growth was typical of ductile fracture initiation characterized by void nucleation, growth and coalescence, in which the initial increments of growth often follow the pattern that is predicted by conventional slip line theory. For tests in the temperature range of 75–125 °C, the formation of flaws which immediately started to blunt was observed, thus creating a new sub-notch. In these cases, no evident crack initiation (in a fracture mechanics point of view) could be observed, and the initial increment of growth follows conventional slip line theory. In this lower temperature range, preliminary stages of both void-coalescence and shear localization initiation could be observed. It should be noted that all test durations were very short compared with the expected service life.

In this context also another test campaign carried out at Swerea KIMAB should be mentioned. The project was about examining the impact of small surface indentations in Cu-OFP (Mannesson and Andersson-Östling 2014) and the results indicate a possible cracking event. When exposing indented specimens for creep it was found small superficial crack formations within and around the indentation. Some findings suggests that it was a surface layer created by spark machining that was cracked, but there is also findings which identifies other cause of events. However, the exact mechanism and root cause is not yet established and more research is needed in order to tell whether there is some connection to the behaviour in CCG. Whether formation of cavities is possible or not at repository temperatures and, if so, if it will lead to the evolution of severe damage within the time horizon of interest is still an open question.

Many different mechanisms can be observed during creep and CCG in Cu-OFP, e.g., cavity formation, blunting, grain boundary sliding, dislocation activity and wedge cracks. It has been seen that cavitation is one common phenomenon for creep and for the CCG of Cu-OFP. However, no distinction can be drawn between the significance and impact of cavities for the different (slow) fracture modes. In this view, a reference campaign with Cu-OF would be important in parallel to Cu-OFP to investigate the difference between certain mechanisms.

As a complement to the review of previous experiments, a small literature survey was conducted with the purpose of identifying relevant fracture mechanisms and models for the two load cases of interest for the deep geological repository. At room temperature and below, copper fails by ductile fracture at high strains to failure, this is virtually insensitive to the applied rate of loading. Well-established fracture models exist for this purpose. At higher temperatures, up to 100 °C, there is experimental evidence that copper may exhibit creep deformation at very low rates. This creep deformation could potentially be a threat to the integrity of the Cu-OFP canister if it was intergranular in nature. If so, the analysis presented by Cocks and Ashby (1982) suggests that it would be caused by cavity growth along grain boundaries that would be driven by surface diffusion influenced by power-law creep. However, the growth rate of such cavities would be so small that they would not lead to failure over the design period of the canister.



## References

SKB's (Svensk Kärnbränslehantering AB) publications can be found at [www.skb.com/publications](http://www.skb.com/publications). SKBdoc documents will be submitted upon request to [document@skb.se](mailto:document@skb.se).

- Anderson T L, 2005.** Fracture mechanics: fundamentals and applications. 3rd ed. Boca Raton, FL, Taylor & Francis.
- Andersson H, 2005.** Creep crack propagation in pure copper at 75 °C. Report IM-2005-130, Corrosion and Metals Research Institute, Sweden.
- Andersson H, Seitisleam F, Sandström R, 1999.** Influence of phosphorous and sulphur as well as grain size on creep in pure copper. SKB TR-99-39, Svensk Kärnbränslehantering AB.
- Argon A S, Hsia K J, Parks D M, 1992.** Growth of cracks by intergranular cavitation in creep. In Argon A S (ed). Topics in fracture and fatigue. Berlin: Springer-Verlag, 146–178.
- Ashby M F, Gandhi C, Taplin D M R, 1979.** Fracture-mechanism maps and their construction for F.C.C. metals and alloys. *Acta Metallurgica* 27, 699–729.
- Ayensu A, Langdon T G, 1996.** The inter-relationship between grain boundary sliding and cavitation during creep of polycrystalline copper. *Metallurgical and Materials Transactions A* 27, 901–907.
- Benzerga A A, Leblond J-B, 2010.** Ductile fracture by void growth and coalescence. *Advances in Applied Mechanics* 44, 169–305.
- Carrecker R P, Hibbard W R, 1953.** Tensile deformation of high-purity copper as a function of temperature, strain rate, and grain size. *Acta Metallurgica* 1, 654–655, 657–663.
- Chuang T-J, Rice J R, 1973.** The shape of intergranular creep cracks growing by surface diffusion. *Acta Metallurgica* 21, 1625–1628.
- Chuang T-J, Kagawa K I, Rice J R, Sills L B, 1973.** Non-equilibrium models for diffuse cavitation of grain interfaces. *Acta Metallurgica* 27, 265–284.
- Cocks A C F, Ashby M F, 1982.** On creep fracture by void growth. *Progress in Material Science* 27, 189–244.
- Fleck R G, Cocks G J, Taplin D M R, 1970.** The influence of polycrystal grain size upon the creep ductility of copper. *Metallurgical Transactions* 1, 3415–3420.
- Gologanu M, Leblond J-B, Perrin G, Devaux J, 1997.** Recent extensions of Gurson's model for porous ductile metals. In Suquet P (ed). *Continuum micromechanics*. Wien: Springer, 61–130.
- Greenwood J N, Miller D R, Suiter J W, 1954.** Intergranular cavitation in stressed metals. *Acta Metallurgica* 2, 250–258.
- Gurson A L, 1977.** Continuum theory of ductile rupture by void nucleation and growth: Part I – Yield criteria and flow rules for porous ductile media. *Journal of Engineering Materials and Technology* 99, 2–15.
- Hayhurst D R, Brown P R, Morrison C J, 1984.** The role of continuum damage in creep crack growth. *Philosophical Transactions of the Royal Society of London A* 311, 131–158.
- Huang Y, 1991.** Accurate dilatation rates for spherical voids in triaxial stress fields. *Journal of Applied Mechanics* 58, 1084–1086.
- Hull D, Rimmer D E, 1959.** The growth of grain-boundary voids under stress. *Philosophical Magazine* 4, 673–687.
- Jenkins W D, Digges T G, 1950.** Creep of high-purity copper. *Journal of Research of the National Bureau of Standards* 45, 153–172.
- Kachanov L M, 1958.** Time of the rupture process under creep conditions (in Russian). *Izvestia Akademii Nauk SSSR, Otdelenie Teckhnicheskikh Nauk* 8, 26–31.
- Kassner M E, Hayes T A, 2003.** Creep cavitation in metals. *International Journal of Plasticity* 19, 1715–1748.

- Lassila D H, 1989.** Effects of grain size and strain rate on the mechanical response of OFHC copper. In Harding J (ed). Mechanical properties of materials at high rates of strain: proceedings of the Fourth International Conference on the Mechanical Properties of Materials at High Rates of Strain, Oxford, 19–22 March 1989, 323–327.
- Leckie F A, Hayhurst D R, 1977.** Constitutive equations for creep rupture. *Acta Metallurgica* 25, 1059–1070.
- Mannesson K, Andersson-Östling H C M, 2014.** Creep of indented copper-cone, sphere and cylinder. KIMAB-2014-114, Swerea KIMAB AB, Sweden. SKBdoc 1442561 ver 1.0, Svensk Kärnbränslehantering AB.
- Miller A G, 1988.** Review of limit-loads of structures containing defects. *International Journal of Pressure Vessels and Piping* 32, 197–327.
- Mirza M S, Barton D C, Church P, Sturges J L, 1997.** Ductile fracture of pure copper: an experimental and numerical study. *Journal de Physique IV*, 891–896.
- Monkman F C, Grant N J, 1956.** An empirical relationship between rupture life and minimum creep rate in creep-rupture tests. *Proceedings of ASTM* 56, 593–620.
- Needleman A, Rice J R, 1980.** Plastic creep flow effects in the diffusive cavitation of grain boundaries. *Acta Metallurgica* 28, 1315–1332.
- Onck P, van der Giessen E, 1998a.** Growth of an initially sharp crack by grain boundary cavitation. *Journal of the Mechanics and Physics of Solids* 47, 99–139.
- Onck P, van der Giessen E, 1998b.** Micromechanics of creep fracture: simulation of intergranular crack growth. *Computational Materials Science* 13, 90–102.
- Pan J, Cocks A C F, 1995.** A numerical technique for the analysis of coupled surface and grain-boundary diffusion. *Acta Metallurgica* 43, 1395–1406.
- Pardoën T, Delannay F, 1998.** Assessment of void growth models from porosity measurements in cold-drawn copper bars. *Metallurgical and Materials Transactions A* 29, 1895–1909.
- Pardoën T, Doghri I, Delannay F, 1998.** Experimental and numerical comparison of void growth models and void coalescence criteria for the prediction of ductile fracture in copper bars. *Acta Metallurgica* 46, 541–552.
- Parry D J, Walker A G, 1989.** Effects of grain size and temperature on mechanical properties of OFHC copper. In Harding J (ed). Mechanical properties of materials at high rates of strain: proceedings of the Fourth International Conference on the Mechanical Properties of Materials at High Rates of Strain, Oxford, 19–22 March 1989, 329–336.
- Rabotnov Y N, 1969.** Creep problems in structural members. Amsterdam: North-Holland.
- Raiko H, Sandström R, Rydén H, Johansson M, 2010.** Design analysis report for the canister. SKB TR-10-28, Svensk Kärnbränslehantering AB.
- Rice J R, Tracy D M, 1969.** On the ductile enlargements of voids in triaxial stress fields. *Journal of the Mechanics and Physics of Solids* 17, 201–217.
- Sandström R, Wu R, 2007.** Origin of the extra low creep ductility of copper without phosphorus. SKB TR-07-02, Svensk Kärnbränslehantering AB.
- Sandström R, Hallgren J, Burman G, 2009.** Stress strain flow curves for Cu-OFP. SKB R-09-14, Svensk Kärnbränslehantering AB.
- Sandström R, Wu R, Hagström J, 2016.** Grain boundary sliding in copper and its relation to cavity formation during creep. *Material Science and Engineering A* 651, 259–268.
- Seitisleam F, Henderson P, 1995.** Creep crack growth in oxygen-free phosphorus copper Cu-OFP (progress report). Report IM-2008-129, Corrosion and Metals Research Institute, Sweden.
- Seitisleam F, Henderson P, 1997.** Creep of copper for nuclear waste containment – results of testing performed in 1996. Report IM-3506, Corrosion and Metals Research Institute, Sweden.

**Tvergaard V, 1981.** Influence of voids on shear band instabilities under plane strain conditions. *International Journal of Fracture* 17, 389–407.

**Wilshire B, 2003.** Knowledge frontiers in strength and fracture of complex creep-resistant alloys. *Strength, Fracture and Complexity* 1, 39–46.

**Wilshire B, Battenbough A J, 2007.** Creep and creep fracture of polycrystalline copper. *Materials Science and Engineering A* 443, 156–166.

**Wu R, Seitisleam F, Sandström R, Jin L-Z, 2011.** Creep crack growth in phosphorus alloyed oxygen free copper. SKB R-11-11, Svensk Kärnbränslehantering AB.

**Wu R, Sandström R, Jin L-Z, 2013.** Creep crack growth in phosphorus alloyed oxygen free copper. *Materials Science and Engineering A* 583, 151–160.

**Yagodzinsky Y, Malitckii E, Saukkonen T, Hänninen H, 2012.** Hydrogen-enhanced creep and cracking of oxygen-free phosphorus-doped copper. *Scripta Materialia* 67, 931–934.

#### **A CO-OPERATION REPORT BETWEEN SVENSK KÄRNBRÄNSLEHANTERING AB AND POSIVA OY**

SKB's and Posiva's programmes both aim at the disposal of spent nuclear fuel based on the KBS-3 concept. Formal cooperation between the companies has been in effect since 2001. In 2014 the companies agreed on extended cooperation where SKB and Posiva share the vision "Operating optimised facilities in 2030". To further enhance the cooperation, Posiva and SKB started a series of joint reports in 2016, which includes this report.